

A theory of representation learning in deep neural networks gives a deep generalisation of kernel methods

Adam X. Yang¹ Maxime Robeyns¹ Edward Milsom¹ Nandi Schoots²
Laurence Aitchison^{1*}

¹University of Bristol ²Kings College London

* Corresponding author: laurence.aitchison@bristol.ac.uk

Abstract

The successes of modern deep neural networks (DNNs) are founded on their ability to transform inputs across multiple layers to build good high-level representations. It is therefore critical to understand this process of representation learning. However, we cannot use standard theoretical approaches involving infinite width limits, as they eliminate representation learning. We therefore develop a new infinite width limit, the representation learning limit, that exhibits representation learning mirroring that in finite-width networks, yet at the same time, remains extremely tractable. For instance, the representation learning limit gives exactly multivariate Gaussian posteriors in deep Gaussian processes with a wide range of kernels, including all isotropic (distance-dependent) kernels. We derive an elegant objective that describes how each network layer learns representations that interpolate between input and output. Finally, we use this limit and objective to develop a flexible, deep generalisation of kernel methods, that we call deep kernel machines (DKMs). We show that DKMs can be scaled to large datasets using methods inspired by inducing point methods from the Gaussian process literature, and we show that DKMs exhibit superior performance to other kernel-based approaches.

1 Introduction

The success of modern deep neural networks (DNNs) is based on their ability to use depth to transform the input into high-level representations that are good for solving difficult tasks [1, 2]. This is particularly evident in settings such as transfer learning, where a model is trained on a large scale dataset such as ImageNet, then the top-layer representation is used to solve a related task [3]. However, the manner in which deep networks learn representations across layers is still poorly understood. In particular, perhaps the key theoretical approach for understanding DNN representations is to take an infinite-width limit [4, 5, 6, 7, 8, 9, 10]. These infinite width limits highlight that representations can be formally described using kernels, which are matrices describing the network’s judgement about the similarity of all pairs of input examples. However, the issue with infinite-width limits is that they eliminate representation learning; instead kernels become deterministic functions of the inputs, and are not learned based on the targets [4, 5, 6, 7, 8, 9, 11, 12, 13]. This is known to compromise performance [8, 13], and is a huge problem if our goal is to understand flexible representation learning in high-performing finite networks. Thus, most work on representation learning sacrifices the theoretical tractability of infinite networks and instead explicitly considers finite networks, and theoretical approaches to finite networks are necessarily complex and approximate e.g. perturbative approaches from statistical physics [14, 15, 16] (also see [17, 18, 19, 20, 21, 22, 23] where these approaches are used to understand other properties of NNs).

We therefore develop a new infinite limit, the “representation learning limit”, which exhibits representation learning mirroring that in finite networks while retaining the theoretical tractability of infinite limits. Formally, we consider a setting where we do gradient descent on the weights while adding IID Gaussian noise, which turns out to be equivalent to placing a prior on the weights of the DNN, and inferring the weights using Bayesian inference [24]. We show that the representations in the

Table 1: Shallow and deep feature-based and kernel-based methods. We introduce deep kernel machines in the lower-right of this table.

| | shallow | deep |
|----------|-------------------------|------------------------------------|
| features | linear regression | deep neural networks (DNNs) |
| kernels | kernel ridge regression | deep kernel machines (DKMs) |

representation learning limit are deterministic and can be obtained by optimizing an objective. This objective has an elegant and easily interpretable form as a chain of KL-divergences that encourage the representations to lie close to those under a randomly initialized infinite network, while at the same time allowing the flexibility to change representations to improve performance (Sec. 2.5). Indeed, in the deep Gaussian process (DGP) setting (which is a deep model exhibiting representation learning similar to that in NNs), the posteriors over features are exactly multivariate Gaussian, and this objective is analytically available, as a sum of KL-divergences of multivariate Gaussians.

DNNs/DGPs in the representation learning limit constitute a new family of machine learning methods that we call deep kernel machines (DKMs). Kernel methods [25, 26, 27] were a leading machine learning approach prior to the deep learning revolution [28]. However, kernel methods were eclipsed by *deep* NNs because depth gives NNs the flexibility to learn a good top-layer representation [13]. In contrast, in a standard kernel method, the kernel (or equivalently the representation) is highly inflexible — there are usually a few tunable hyperparameters, but nothing that approaches the enormous flexibility of the top-layer representation in a DNN. DKMs are the first deep generalisation of kernel methods that work entirely with kernels that give flexibility comparable to that in DNNs. We show that DKMs can be combined with scaling methods from the DGP literature, resulting in an effective, scalable approach that improves over alternatives, such as simply optimizing the hyperparameters of the kernel, or doing maximum *a-posterior* inference on the features.

2 Results

2.1 A general model containing DNNs and DGPs

We start by defining a unified deep model that contains both DGPs and DNNs as special cases. In particular, our model contains DNNs with an IID Gaussian prior over the weights (Appendix B, which is equivalent to non-Bayesian network where we add Gaussian noise during training [24]). This model maps from inputs, $\mathbf{X} \in \mathbb{R}^{P \times \nu_0}$, to outputs, $\mathbf{Y} \in \mathbb{R}^{P \times \nu_{L+1}}$, where P is the number of input points, ν_0 is the number of input features, and ν_{L+1} is the number of output features. The model has L intermediate layers, indexed $\ell \in \{1, \dots, L\}$, and at each intermediate layer there are N_ℓ features, $\mathbf{F}_\ell \in \mathbb{R}^{P \times N_\ell}$. The features, \mathbf{F}_ℓ , and outputs, \mathbf{Y} , can be written as a stack of vectors,

$$\mathbf{F}_\ell = (\mathbf{f}_1^\ell \quad \mathbf{f}_2^\ell \quad \dots \quad \mathbf{f}_{N_\ell}^\ell) \quad \mathbf{Y} = (\mathbf{y}_1 \quad \mathbf{y}_2 \quad \dots \quad \mathbf{y}_{\nu_{L+1}}),$$

where $\mathbf{f}_\lambda^\ell \in \mathbb{R}^P$ gives the value of one feature and $\mathbf{y}_\lambda \in \mathbb{R}^P$ gives the value of one output for all P input points. The features, $\mathbf{F}_1, \dots, \mathbf{F}_L$, and (for regression) the outputs, \mathbf{Y} , are sampled from a Gaussian process (GP) with a covariance or kernel determined by the features at the previous layer (Fig. 1 top),

$$\mathbb{P}(\mathbf{F}_\ell | \mathbf{F}_{\ell-1}) = \prod_{\lambda=1}^{N_\ell} \mathcal{N}(\mathbf{f}_\lambda^\ell; \mathbf{0}, \mathbf{K}(\mathbf{G}(\mathbf{F}_{\ell-1}))) \quad (1a)$$

$$\mathbb{P}(\mathbf{Y} | \mathbf{F}_L) = \prod_{\lambda=1}^{\nu_{L+1}} \mathcal{N}(\mathbf{y}_\lambda; \mathbf{0}, \mathbf{K}(\mathbf{G}(\mathbf{F}_L)) + \sigma^2 \mathbf{I}). \quad (1b)$$

Note we only use the regression likelihood to give a concrete example; we could equally use an alternative likelihood e.g. for classification (Appendix A).

The distinction between a DNN and a DGP emerges only in the choice of kernel, $\mathbf{K}(\mathbf{G}(\mathbf{F}_{\ell-1}))$ (we will discuss the distinction between $\mathbf{K}(\cdot)$ and $\mathbf{G}(\cdot)$ in the next paragraph). For a DNN the kernel that arises when you integrate the IID Gaussian prior on weights is the outer product of the NN nonlinearity, ϕ , applied to all feature vectors (Appendix B),

$$\mathbf{K}_{\text{DNN}}(\mathbf{G}_{\text{DNN}}(\mathbf{F}_{\ell-1})) = \frac{1}{N_{\ell-1}} \sum_{\lambda=1}^{N_{\ell-1}} \phi(\mathbf{f}_\lambda^{\ell-1}) \phi^T(\mathbf{f}_\lambda^{\ell-1}), \quad (2)$$

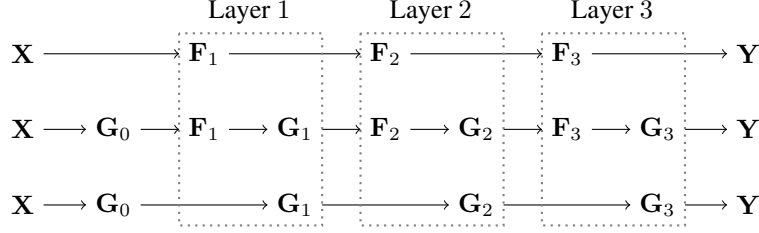


Figure 1: The graphical model structure for each of our generative models for $L = 3$. **Top.** The standard model (Eq. 1), written purely in terms of features, \mathbf{F}_ℓ . **Middle.** The standard model, including Gram matrices as random variables (Eq. 6) **Bottom.** Integrating out the activations, \mathbf{F}_ℓ ,

For a DGP, we choose the kernel to be an isotropic kernel which depends only on the distance, such as squared exponential [29], or a non-isotropic kernel such as an arccos kernel used in the infinite NN literature [30].

We split the computation of the kernel into the application of two functions, $\mathbf{K}(\cdot)$ and $\mathbf{G}(\cdot)$. While this split is not necessary to define the DNN and DGP priors, it exposes the empirical average over feature vectors that is present in both DNNs and DGPs, and which turns out to be critical to all our theoretical analyses. In particular, we define the Gram matrix, $\mathbf{G}(\mathbf{F}_\ell) \in \mathbb{R}^{P \times P}$, to be

$$\mathbf{G}_{\text{DNN}}(\mathbf{F}_{\ell-1}) = \frac{1}{N_{\ell-1}} \sum_{\lambda=1}^{N_{\ell-1}} \phi(\mathbf{f}_\lambda^{\ell-1}) \phi^T(\mathbf{f}_\lambda^{\ell-1}), \quad (3a)$$

$$\mathbf{G}_{\text{DGP}}(\mathbf{F}_{\ell-1}) = \frac{1}{N_{\ell-1}} \sum_{\lambda=1}^{N_{\ell-1}} \mathbf{f}_\lambda^{\ell-1} (\mathbf{f}_\lambda^{\ell-1})^T. \quad (3b)$$

We then apply a function, $\mathbf{K}(\cdot)$, which transforms the Gram matrix to the final kernel.

$$\mathbf{K}_{\text{DNN}}(\mathbf{G}_{\ell-1}) = \mathbf{G}_{\ell-1}, \quad (4a)$$

$$K_{\text{isotropic};ij}(\mathbf{G}_{\ell-1}) = k_{\text{isotropic}}(R_{ij}(\mathbf{G}_{\ell-1})) \quad (4b)$$

For DNNs, $\mathbf{K}_{\text{DNN}}(\cdot)$ is the identity, so that combining Eq. (3a) with Eq. (4a) gives Eq. (2). For DGPs, this is where we compute the kernel. Here, we give an example for isotropic kernels such as the squared exponential which depend on the (normalized) squared distance, R_{ij} (see Eq. 5). This approach of computing the kernel from the Gram matrix might seem strange, because kernels are usually computed from features. However, it turns out that almost all standard kernels used in the GP literature depend on the features only through the Gram matrix. This includes all isotropic kernels that depend on distance, but also non-isotropic kernels such as the arccos kernels used in the infinite neural network literature [30]. Isotropic kernels work because the (normalized) squared distance, $R_{ij}(\mathbf{G})$, can be computed from the Gram matrix,

$$\begin{aligned} R_{ij}(\mathbf{G}) &= \frac{1}{N} \sum_{\lambda=1}^N (F_{i\lambda} - F_{j\lambda})^2 = \frac{1}{N} \sum_{\lambda=1}^N ((F_{i\lambda})^2 - 2F_{i\lambda}F_{j\lambda} + (F_{j\lambda})^2) \\ &= G_{ii} - 2G_{ij} + G_{jj} \end{aligned} \quad (5)$$

where λ indexes features, i and j index datapoints and we have omitted the layer index to simplify the equation (for further details, see [31]).

2.2 DNN and DGP generative models can be written purely in terms of Gram matrices

Notice that \mathbf{F}_ℓ depends on $\mathbf{F}_{\ell-1}$ only through $\mathbf{G}(\mathbf{F}_{\ell-1})$, and \mathbf{Y} depends on \mathbf{F}_L only through $\mathbf{G}(\mathbf{F}_L)$ (Eq. 1). We can therefore introduce random variables representing the Gram matrices, $\mathbf{G}_\ell = \mathbf{G}(\mathbf{F}_\ell)$, where \mathbf{G}_ℓ is a random variable representing the Gram matrix at layer ℓ , whereas $\mathbf{G}(\cdot)$ is a function that takes features and computes the corresponding Gram matrix. The generative model can then be rewritten in terms of the Gram matrices (Fig. 1 middle),

$$P(\mathbf{F}_\ell | \mathbf{G}_{\ell-1}) = \prod_{\lambda=1}^{N_\ell} \mathcal{N}(\mathbf{f}_\lambda^\ell; \mathbf{0}, \mathbf{K}(\mathbf{G}_{\ell-1})), \quad (6a)$$

$$P(\mathbf{G}_\ell | \mathbf{F}_\ell) = \delta(\mathbf{G}_\ell - \mathbf{G}(\mathbf{F}_\ell)) \quad (6b)$$

$$P(\mathbf{Y} | \mathbf{G}_L) = \prod_{\lambda=1}^{\nu_L+1} \mathcal{N}(y_\lambda; \mathbf{0}, \mathbf{K}(\mathbf{G}_L) + \sigma^2 \mathbf{I}). \quad (6c)$$

where δ is the Dirac-delta, and e.g. $\mathbf{G}_0 = \frac{1}{\nu_0} \mathbf{X}\mathbf{X}^T$. Again, for concreteness we have used a regression likelihood, but other likelihoods could also be used.

Now, we can integrate \mathbf{F}_ℓ out of the model, in which case, we get an equivalent generative model written solely in terms of Gram matrices (Fig. 1 bottom), with

$$P(\mathbf{G}_\ell | \mathbf{G}_{\ell-1}) = \int d\mathbf{F}_\ell P(\mathbf{G}_\ell | \mathbf{F}_\ell) P(\mathbf{F}_\ell | \mathbf{G}_{\ell-1}), \quad (7)$$

and with the usual likelihood (e.g. Eq. 6c). While we can write down this generative model, actually finding $P(\mathbf{G}_\ell | \mathbf{G}_{\ell-1})$ by evaluating this integral analytically is not possible in general. However, for one special case, an analytic form is available. In particular, for DGPs note that the Gram matrix (Eq. 3b) is the outer product of IID Gaussian distributed vectors (Eq. 1a). This matches the definition of the well-known Wishart distribution, so we have,

$$P_{\text{DGP}}(\mathbf{G}_\ell | \mathbf{G}_{\ell-1}) = \text{Wishart}\left(\mathbf{G}_\ell; \frac{1}{N_\ell} \mathbf{K}(\mathbf{G}_{\ell-1}), N_\ell\right) \quad (8)$$

$$\log P_{\text{DGP}}(\mathbf{G}_\ell | \mathbf{G}_{\ell-1}) = \frac{N_\ell - P - 1}{2} \log |\mathbf{G}_\ell| - \frac{N_\ell}{2} \log |\mathbf{K}(\mathbf{G}_{\ell-1})| - \frac{N_\ell}{2} \text{Tr}(\mathbf{K}^{-1}(\mathbf{G}_{\ell-1}) \mathbf{G}_\ell) + \text{const.}$$

This distribution over Gram matrices is valid for DGPs of any width. However, in more general cases including BNNs no such analytic form is available; instead, to make progress we need to consider the limit of an infinitely wide network. Thus, in the next two sections, we give the standard infinite width limit, show that it is flawed because it eliminates representation learning, then introduce our DKM limit which retains representation learning.

2.3 Standard infinite width limits of DNNs and DGPs lack representation learning

We are now in a position to take a new approach to deriving past results (e.g. [6, 7, 9, 8]) on infinitely wide DNN/DGPs. In particular, the standard infinite width limit is,

$$N_\ell = N \nu_\ell \quad \text{for} \quad \ell \in \{1, \dots, L\} \quad \text{with} \quad N \rightarrow \infty. \quad (9)$$

The log-posterior is,

$$\log P(\mathbf{G}_1, \dots, \mathbf{G}_L | \mathbf{X}, \mathbf{Y}) = \log P(\mathbf{Y} | \mathbf{G}_L) + \sum_{\ell=1}^L \log P(\mathbf{G}_\ell | \mathbf{G}_{\ell-1}) + \text{const.} \quad (10)$$

Now, we can consider the log-posterior in the limit as $N \rightarrow \infty$. The log-prior, $\log P(\mathbf{G}_\ell | \mathbf{G}_{\ell-1})$, scales with N . To get a finite limit, we therefore need to divide by N , and it turns out this limit can be written as the KL-divergence between two multivariate Gaussians,

$$\begin{aligned} \lim_{N \rightarrow \infty} \frac{1}{N} \log P_{\text{DGP}}(\mathbf{G}_\ell | \mathbf{G}_{\ell-1}) &= -\frac{\nu_\ell}{2} (\log |\mathbf{K}(\mathbf{G}_{\ell-1}) \mathbf{G}_\ell| - \text{Tr}(\mathbf{K}^{-1}(\mathbf{G}_{\ell-1}) \mathbf{G}_\ell)) + \text{const} \\ &= -\nu_\ell D_{\text{KL}}(\mathcal{N}(\mathbf{0}, \mathbf{G}_\ell) \| \mathcal{N}(\mathbf{0}, \mathbf{K}(\mathbf{G}_{\ell-1}))) + \text{const.} \end{aligned} \quad (11)$$

In contrast, the log likelihood, $\log P(\mathbf{Y} | \mathbf{G}_L)$, is constant wrt N (Eq. 6c), so $\lim_{N \rightarrow \infty} \frac{1}{N} \log P(\mathbf{Y} | \mathbf{G}_L) = 0$. The limiting log-posterior is thus,

$$\lim_{N \rightarrow \infty} \frac{1}{N} \log P_{\text{DGP}}(\mathbf{G}_1, \dots, \mathbf{G}_L | \mathbf{X}, \mathbf{Y}) = -\sum_{\ell=1}^L \nu_\ell D_{\text{KL}}(\mathcal{N}(\mathbf{0}, \mathbf{G}_\ell) \| \mathcal{N}(\mathbf{0}, \mathbf{K}(\mathbf{G}_{\ell-1}))) + \text{const.} \quad (12)$$

This form highlights that the log-posterior scales with N , so in the limit as $N \rightarrow \infty$, the posterior converges to a point distribution concentrated around the global maximum, denoted $\mathbf{G}_1^*, \dots, \mathbf{G}_L^*$, (see Appendix C for a formal discussion of weak convergence),

$$\lim_{N \rightarrow \infty} P(\mathbf{G}_1, \dots, \mathbf{G}_L | \mathbf{X}, \mathbf{Y}) = \prod_{\ell=1}^L \delta(\mathbf{G}_\ell - \mathbf{G}_\ell^*). \quad (13)$$

Moreover, it is evident from the KL-divergence form for the log-posterior (Eq. 12) that the unique global maximum can be computed recursively as $\mathbf{G}_\ell^* = \mathbf{K}(\mathbf{G}_{\ell-1}^*)$, with $\mathbf{G}_0^* = \frac{1}{\nu_0} \mathbf{X} \mathbf{X}^T$. Thus, the limiting posterior over Gram matrices does not depend on the training targets, so there is no possibility of representation learning [13]. This is deeply problematic: as described earlier, the point of deep learning is to flexibly learn top-layer features or representations that give good performance.

2.4 The representation learning limit

The key issue with standard infinite width limits was that as we took $N \rightarrow \infty$ the log-prior terms, $\log P(\mathbf{G}_\ell | \mathbf{G}_{\ell-1})$, in Eq. (10) dominated the log-likelihood, $\log P(\mathbf{Y} | \mathbf{G}_L)$, eliminating representation learning. In contrast, we introduce the ‘‘representation learning limit’’ which retains representation

learning. In particular, the representation learning limit ensures the likelihood is not dominated by the prior terms by sending the number of output features, N_{L+1} , to infinity as the layer-widths go to infinity,

$$N_\ell = N \nu_\ell \quad \text{for} \quad \ell \in \{1, \dots, L+1\} \quad \text{with} \quad N \rightarrow \infty. \quad (14)$$

Importantly, the representation learning limit gives a valid probabilistic model with a well-defined posterior, arising from our usual prior, (e.g. Eq. 7) and a likelihood, which assumes each output channel is IID,

$$P(\tilde{\mathbf{Y}}|\mathbf{G}_L) = \prod_{\lambda=1}^{N_{L+1}} \mathcal{N}(\tilde{\mathbf{y}}_\lambda; \mathbf{0}, \mathbf{K}(\mathbf{G}_L) + \sigma^2 \mathbf{I}). \quad (15)$$

where $\tilde{\mathbf{Y}} \in \mathbb{R}^{P \times N_{L+1}}$ is infinite width (Eq. 14) whereas the usual DGP data, $\mathbf{Y} \in \mathbb{R}^{P \times \nu_{L+1}}$, is finite width. Of course, infinite-width data is unusual if not unheard-of; in practice, real data, $\mathbf{Y} \in \mathbb{R}^{P \times \nu_{L+1}}$, almost always has a finite number of features, ν_{L+1} . How do we apply the DKM to such data? The answer is to define $\tilde{\mathbf{Y}}$ as N IID copies of the underlying data, \mathbf{Y} , i.e. $\tilde{\mathbf{Y}} = (\mathbf{Y} \ \cdots \ \mathbf{Y})$, which implies that the likelihood in the representation learning limit is N times larger than the usual likelihood,

$$\log P(\tilde{\mathbf{Y}}|\mathbf{G}_L) = N \log P(\mathbf{Y}|\mathbf{G}_L). \quad (16)$$

This allows us to retain \mathbf{Y} dependence in the posterior and hence representation learning even with an infinitely wide network.

The log-posterior in the representation learning limit is very similar to the log-posterior in the standard limit (Eq. 12). The only difference is that the likelihood, $\log P(\tilde{\mathbf{Y}}|\mathbf{G}_L)$ now scales with N , so it does not disappear as we take the limit,

$$\begin{aligned} \mathcal{L}(\mathbf{G}_1, \dots, \mathbf{G}_L) &= \lim_{N \rightarrow \infty} \frac{1}{N} \log P(\mathbf{G}_1, \dots, \mathbf{G}_L | \mathbf{X}, \tilde{\mathbf{Y}}) + \text{const}, \\ &= \log P(\mathbf{Y}|\mathbf{G}_L) - \sum_{\ell=1}^L \nu_\ell \text{D}_{\text{KL}}(\mathcal{N}(\mathbf{0}, \mathbf{G}_\ell) \| \mathcal{N}(\mathbf{0}, \mathbf{K}(\mathbf{G}_{\ell-1}))). \end{aligned} \quad (17)$$

Here, we denote the limiting log-posterior as $\mathcal{L}(\mathbf{G}_1, \dots, \mathbf{G}_L)$, and we call this the DKM objective, as the representation learning limit results in a practical method, called the deep kernel machine, or DKM, which uses this objective and which we introduce later (Sec. 2.8). The inclusion of the likelihood term means that the global optimum $\mathbf{G}_1^*, \dots, \mathbf{G}_L^*$ cannot be computed directly, instead we need to explicitly optimize. The posterior converges to a point distribution as long as the global maximum of $\mathcal{L}(\mathbf{G}_1, \dots, \mathbf{G}_L)$ is unique, (allowing any number of local maxima, as long as they all lie below the global maximum). Unlike in the standard limit (Eq. 12), it is no longer possible to guarantee uniqueness of the global maximum. However, we do expect the global maximum to be unique in most practical settings: we know the maximum is unique when the prior dominates (Eq. 12), in Appendix I, we prove uniqueness for linear models, and in Sec. J, we give a number of experiments in nonlinear models in which optimizing from very different initializations found the same maximum, indicating uniqueness in practical settings.

So far, we only gave the DKM objective for DGPs (Eq. 17). To get a more general form, we need to consider the implied posteriors over features. In particular, the posterior over features conditioned on Gram matrices is IID over features (Appendix D.1), $\mathbf{f}_1^\ell, \dots, \mathbf{f}_{N_\ell}^\ell$ and for DGPs, it is multivariate Gaussian (Appendix D.2),

$$P(\mathbf{F}_\ell | \mathbf{G}_{\ell-1}, \mathbf{G}_\ell) = \prod_{\lambda=1}^{N_\ell} P(\mathbf{f}_\lambda^\ell | \mathbf{G}_{\ell-1}, \mathbf{G}_\ell) \underset{\text{for DGPs}}{=} \prod_{\lambda=1}^{N_\ell} \mathcal{N}(\mathbf{f}_\lambda^\ell; \mathbf{0}, \mathbf{G}_\ell). \quad (18)$$

If $\mathcal{L}(\mathbf{G}_1, \dots, \mathbf{G}_L)$ has a single global optimum, so the posterior over Gram matrices converges to a point at $\mathbf{G}_1^*, \dots, \mathbf{G}_L^*$, the full posterior over features becomes,

$$P(\mathbf{F}_1, \dots, \mathbf{F}_L | \mathbf{X}, \mathbf{Y}) = \prod_{\ell=1}^L \prod_{\lambda=1}^{N_\ell} P(\mathbf{f}_\lambda^\ell | \mathbf{G}_{\ell-1}^*, \mathbf{G}_\ell^*) \underset{\text{for DGPs}}{=} \prod_{\ell=1}^L \prod_{\lambda=1}^{N_\ell} \mathcal{N}(\mathbf{f}_\lambda^\ell; \mathbf{0}, \mathbf{G}_\ell^*). \quad (19)$$

Now, we can see that Eq. (17) is a specific example of a general expression. In particular, note that the distribution on the right of the KL-divergence in Eq. (17) is the DGP posterior over features (Eq. 18). Thus, the DKM objective can alternatively be written,

$$\mathcal{L}(\mathbf{G}_1, \dots, \mathbf{G}_L) = \log P(\mathbf{Y}|\mathbf{G}_L) - \sum_{\ell=1}^L \nu_\ell \text{D}_{\text{KL}}(P(\mathbf{f}_\lambda^\ell | \mathbf{G}_{\ell-1}, \mathbf{G}_\ell) \| \mathcal{N}(\mathbf{0}, \mathbf{K}(\mathbf{G}_{\ell-1}))), \quad (20)$$

And this form holds for all models in our class, including BNNs (Appendix D.3). As in DGPs, the log-posterior is N times $\mathcal{L}(\mathbf{G}_1, \dots, \mathbf{G}_L)$ (Eq. 17), so as N is taken to infinity, the posterior for all models becomes a point distribution (Eq. 13) around the unique global maximum of $\mathcal{L}(\mathbf{G}_1, \dots, \mathbf{G}_L)$, denoted $\mathbf{G}_1^*, \dots, \mathbf{G}_L^*$.

2.5 Using the DKM objective to understand representation learning

The form for the DKM objective in Eq. (20) gives a strong intuition for how representation learning occurs in deep networks. It is perhaps easiest to consider the DGP case (Eq. 17), where the DKM objective simply consists of KL-divergences of multivariate Gaussians with covariances \mathbf{G}_ℓ and $\mathbf{K}(\mathbf{G}_{\ell-1})$. Critically, these KL-divergences act as a strong regulariser, encouraging \mathbf{G}_ℓ to lie close to $\mathbf{K}(\mathbf{G}_{\ell-1})$, their value under the infinite DGP prior (Sec. 2.3). At the same time, the likelihood, $\log P(\mathbf{Y}|\mathbf{G}_L)$, encourages the model to find a representation giving good performance on the training data. We could use any form for the likelihood including classification and regression, but to understand how the likelihood interacts with the other KL-divergence terms, it is easiest to consider regression (Eq. 6c), as this log-likelihood can be written as a KL-divergence,

$$\log P(\mathbf{Y}|\mathbf{G}_L) = -\nu_{L+1} \text{D}_{\text{KL}}(\mathcal{N}(\mathbf{0}, \mathbf{G}_{L+1}) \parallel \mathcal{N}(\mathbf{0}, \mathbf{K}(\mathbf{G}_L) + \sigma^2 \mathbf{I})) + \text{const} \quad (21)$$

Thus, the likelihood encourages $\mathbf{K}(\mathbf{G}_L) + \sigma^2 \mathbf{I}$ to be as possible to the covariance of the data, $\mathbf{G}_{L+1} = \frac{1}{\nu_{L+1}} \mathbf{Y}\mathbf{Y}^T$, while the DGP prior terms encourage all \mathbf{G}_ℓ to lie close to $\mathbf{K}(\mathbf{G}_{\ell-1})$. In combination, we would expect the optimal Gram matrices to “interpolate” between the input kernel, $\mathbf{G}_0 = \frac{1}{\nu_0} \mathbf{X}\mathbf{X}^T$ and the output kernel, \mathbf{G}_{L+1} . To make the notion of interpolation explicit, we consider $\sigma^2 = 0$ with a linear kernel, $\mathbf{K}(\mathbf{G}_{\ell-1}) = \mathbf{G}_{\ell-1}$, so named because it corresponds to a linear neural network layer. With this kernel and with all $\nu_\ell = \nu$, there is an analytic solution for the (unique) optimum of the DKM objective (Appendix I.1),

$$\mathbf{G}_\ell^* = \mathbf{G}_0 (\mathbf{G}_0^{-1} \mathbf{G}_{L+1})^{\ell/(L+1)}, \quad (22)$$

Of course, this discussion was primarily for DGPs, but the exact same intuitions hold in general, e.g. for DNNs, in that maximizing the DKM objective finds a sequence of Gram matrices, $\mathbf{G}_1^*, \dots, \mathbf{G}_L^*$ that interpolate between the input kernel, \mathbf{G}_0 and the output kernel, \mathbf{G}_{L+1} . The only difference is in details of $P(\mathbf{G}_\ell|\mathbf{G}_{\ell-1})$, which arise as details of how the KL-divergences in the DKM objective are specified.

2.6 Approximating the DNN DKM objective

In practice, the true posteriors required to evaluate Eq. (20) are intractable for DNNs, raising the question of how to develop accurate approximations for DNNs. There is a path to developing a variational DKM objective by taking inspiration from variational inference [32, 33]. The variational DKM objective is written in terms of a variational approximate posterior, $Q_{\theta_\ell}(\mathbf{f}_\lambda^\ell)$ with parameters θ_ℓ (Appendix D.4), which is designed to mirror the true posterior. We can use the approximate posterior to bound the KL-divergences in the DKM objective,

$$-\text{D}_{\text{KL}}(P(\mathbf{f}_\lambda^\ell|\mathbf{G}_{\ell-1}, \mathbf{G}_\ell = \mathbf{G}_\theta(\theta_\ell)) \parallel P(\mathbf{f}_\lambda^\ell|\mathbf{G}_{\ell-1})) \geq -\text{D}_{\text{KL}}(Q_{\theta_\ell}(\mathbf{f}_\lambda^\ell) \parallel P(\mathbf{f}_\lambda^\ell|\mathbf{G}_{\ell-1})). \quad (23)$$

The bound is tight when the approximate posterior equals the true posterior. Importantly, this only allows us to bound the KL-divergence for the specific Gram matrix, \mathbf{G}_ℓ , implied by the approximate posterior,

$$\mathbf{G}_\theta(\theta_\ell) = \mathbb{E}_{Q_{\theta_\ell}(\mathbf{f}_\lambda^\ell)} [\phi(\mathbf{f}_\lambda^\ell) \phi^T(\mathbf{f}_\lambda^\ell)]. \quad (24)$$

For some combinations of approximate posterior and nonlinearity, we may have an analytic form for $\mathbf{G}_\theta(\theta_\ell)$, but we can always approximate $\mathbf{G}_\theta(\theta_\ell)$ using Monte Carlo sampling (i.e. sampling a large number of \mathbf{f}_λ^ℓ from $Q_{\theta_\ell}(\mathbf{f}_\lambda^\ell)$ and computing the average of the resulting $\phi(\mathbf{f}_\lambda^\ell) \phi^T(\mathbf{f}_\lambda^\ell)$). While it might seem restrictive to only be able to evaluate the KL-divergence at $\mathbf{G}_\theta(\theta_\ell)$, in practice, we are going to want to optimize over Gram matrices to find the maximum of the DKM objective. In that case, we can just switch from optimizing Gram matrices, $\mathbf{G}_1, \dots, \mathbf{G}_L$, directly to optimizing approximate posterior parameters, $\theta_1, \dots, \theta_L$ and then computing the implied Gram matrices using Eq. (24). In particular, we optimize the approximate posterior parameters using the variational DKM objective,

$$\mathcal{L}_V(\theta_1, \dots, \theta_L) = \log P(\mathbf{Y}|\mathbf{G}_\theta(\theta_L)) - \sum_{\ell=1}^L \nu_\ell \text{D}_{\text{KL}}(Q_{\theta_\ell}(\mathbf{f}_\lambda^\ell) \parallel \mathcal{N}(\mathbf{0}, \mathbf{K}(\mathbf{G}_\theta(\theta_{\ell-1})))), \quad (25)$$

which bounds the true DKM objective,

$$\mathcal{L}(\mathbf{G}_\theta(\theta_1), \dots, \mathbf{G}_\theta(\theta_L)) \geq \mathcal{L}_V(\theta_1, \dots, \theta_L), \quad (26)$$

with equality when the approximate posteriors, $Q_{\theta_\ell}(\mathbf{f}_\lambda^\ell)$, equal the true posteriors, $P(\mathbf{f}_\lambda^\ell|\mathbf{G}_{\ell-1}, \mathbf{G}_\ell)$.

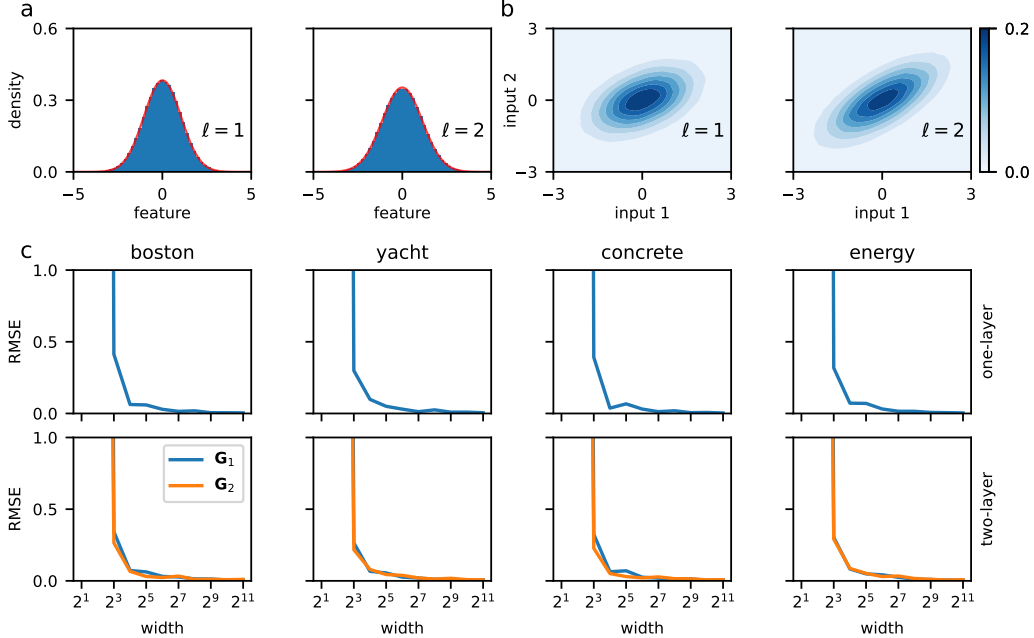


Figure 2: Wide DGP posteriors converge to the DKM. Here, we trained DGPs with Langevin dynamics (see Methods), and compared to matched trained DKM. **a** Marginal distribution over features for one input datapoint for a two-layer DGP trained on a subset of yacht. We used a width of $N_{1\dots L} = 1024$ and $\nu_{1\dots L} = 5$ in all plots to ensure that the data had a strong effect on the learned representations. The marginals (blue histogram) are very close to Gaussian (the red line shows the closest fitted Gaussian). Remember that the true posterior over features is IID (Eq. 19), so each column aggregates the distribution over features (and over 10 parallel chains with 100 samples from each chain) for a single input datapoint. **b** The 2D marginal distributions for the same DGP for two input points (horizontal and vertical axes). **c** Element-wise RMSE (normalized Frobenius distance) between Gram matrices from a trained DKM compared to trained DGPs of increasing width. The DGP Gram matrices converge to the DKM solution as width becomes larger.

2.7 The DKM objective captures observed representation learning in finite networks

DKMs thus give strong insight into representation learning. Here, we confirm that these insights apply to representation learning in finite networks. We begin by touching on two theoretical results that we give in full in the Appendix. First, we find that the representations learned by MAP inference over DGP features (rather than Gram matrices as we consider in the main text) gives exactly the same solution for any N (finite or infinite; Appendix E.1). Second, in Appendix E.2, we find that Langevin dynamics for the DKM posterior are deterministic, equivalent to preconditioned gradient descent on the DKM objective, and equivalent to the expected Langevin updates to the Gram matrices for a finite-width DGP.

Next, we confirmed the similarity of finite and infinite width networks experimentally, doing inference in finite-width DGPs using Langevin sampling (see Methods for details). We began by confirming that the DGP posteriors are Gaussian (Eq. 19; Fig. 2ab). Next, we confirmed that the representations match closely for infinite-width DKMs (Fig. 3 top and bottom rows) and finite-width DGPs (Fig. 3 middle two rows), both at initialization (Fig. 3 top two rows) and after training to convergence (Fig. 3 bottom two rows). Note that the first column, \mathbf{K}_0 is a squared exponential kernel applied to the input data, and $\mathbf{G}_3 = \mathbf{y}\mathbf{y}^T$ is the output Gram matrix (in this case, there is only one output feature).

To understand the quality of the match for different network widths, and datasets, we considered the RMSE (equivalently the normalized Frobenius norm) between elements of the Gram matrices for networks of different widths (x-axis) for different UCI datasets (columns) and different numbers of layers (top row is one-layer, bottom row is two-layers; Fig. 2c). In most cases, we found a good

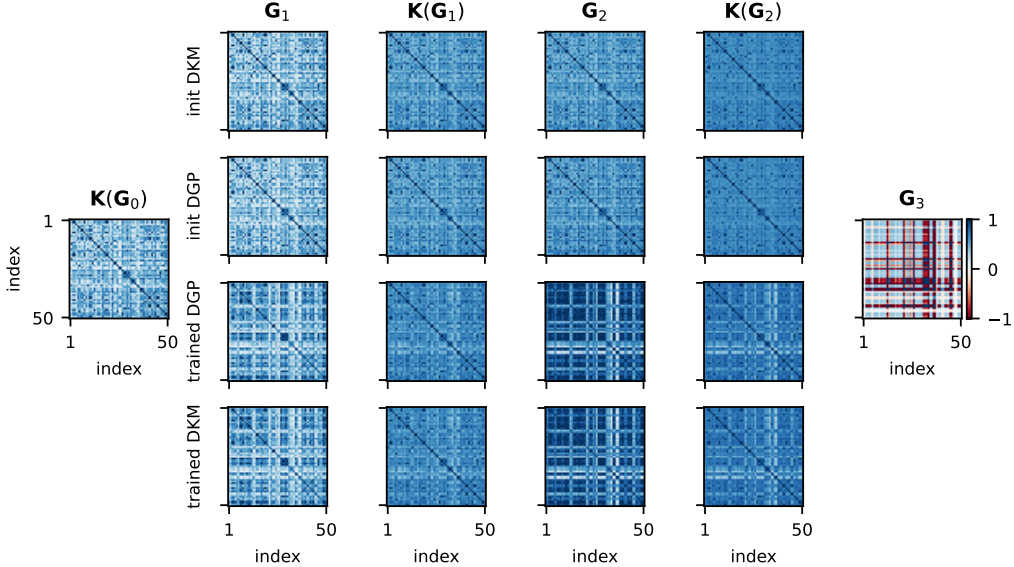


Figure 3: A two hidden layer DGP with 1024 units per hidden layer and DKM with squared exponential kernels match closely. The data was the first 50 datapoints of the yacht dataset. The first column, \mathbf{K}_0 is a fixed squared exponential kernel applied to the inputs, and the last column, $\mathbf{G}_3 = \mathbf{y}\mathbf{y}^T$ is the fixed output Gram matrix. The first row is the DKM initialization at the prior Gram matrices and kernels, and the second row is the DGP, which is initialized by sampling from the prior. As expected, the finite width DGP prior closely matches the infinite-width DKM initialization, which corresponds to the standard infinite width limit. The third row is the Gram matrices and kernels for the trained DGP, which has changed dramatically relative to its initialization (second row) in order to better fit the data. The fourth row is the Gram matrices and kernels for the optimized DKM, which closely matches those for the trained DGP.

match as long as the width was at least 128, which is around the width of typical fully connected neural network, albeit a little larger than the typical width of DGPs (e.g. [34]).

Next, we consider the match for DNNs. This is a bit more involved, as the marginal distributions over features are no longer Gaussian (Fig. 4b). To capture these non-Gaussian marginals, we used a very simple normalizing flow, by first sampling \mathbf{z}_λ^ℓ from a multivariate Gaussian with a learned mean, $\boldsymbol{\mu}_\ell$, then passing those \mathbf{z}_λ^ℓ through a learned pointwise function, $\mathbf{f}(\cdot)$, parameterised by a quadratic spline as in neural spline flow [35],

$$\mathbf{z}_\lambda^\ell \sim \mathcal{N}(\boldsymbol{\mu}_\ell, \boldsymbol{\Sigma}_\ell) \quad \mathbf{f}_\lambda^\ell = \mathbf{f}(\mathbf{z}_\lambda^\ell) \quad (27)$$

The resulting distribution is exactly that in a high-dimensional Gaussian copula (e.g. [36]). As shown in Fig. 4, vDKM with multivariate Gaussian (MvG) approximate posterior cannot match the Gram matrices learned by DNN (Fig. 4a), while vDKM with flow is able to capture the non-Gaussian marginals (Fig. 4b) and thus match the learned Gram matrices with DNN.

2.8 Practical learning in the representation learning limit with DKMs

Here, we compare the performance of the deep kernel machine objective (Eq. 17) and MAP over features (Sec. E.1) for DGPs. In addition, we considered a baseline, which was a standard, shallow kernel method mirroring the structure of the deep kernel machine but where the only flexibility comes from the hyperparameters. Formally, this model can be obtained by setting, $\mathbf{G}_\ell = \mathbf{K}(\mathbf{G}_{\ell-1})$ and is denoted “Kernel Hyper” in Table 2.

We applied these methods to UCI datasets [37]. We used a two hidden layer architecture, with a kernel inspired by the skip-connections used in DGPs [34], $\mathbf{K}(\mathbf{G}_\ell) = w_1^\ell \mathbf{G}_\ell + w_2^\ell \mathbf{K}_{\text{sqexp}}(\mathbf{G}_\ell)$, where w_1^ℓ , w_2^ℓ and σ are hyperparameters, and $\mathbf{K}_{\text{sqexp}}(\mathbf{G}_\ell)$ is a standard squared-exponential kernel.

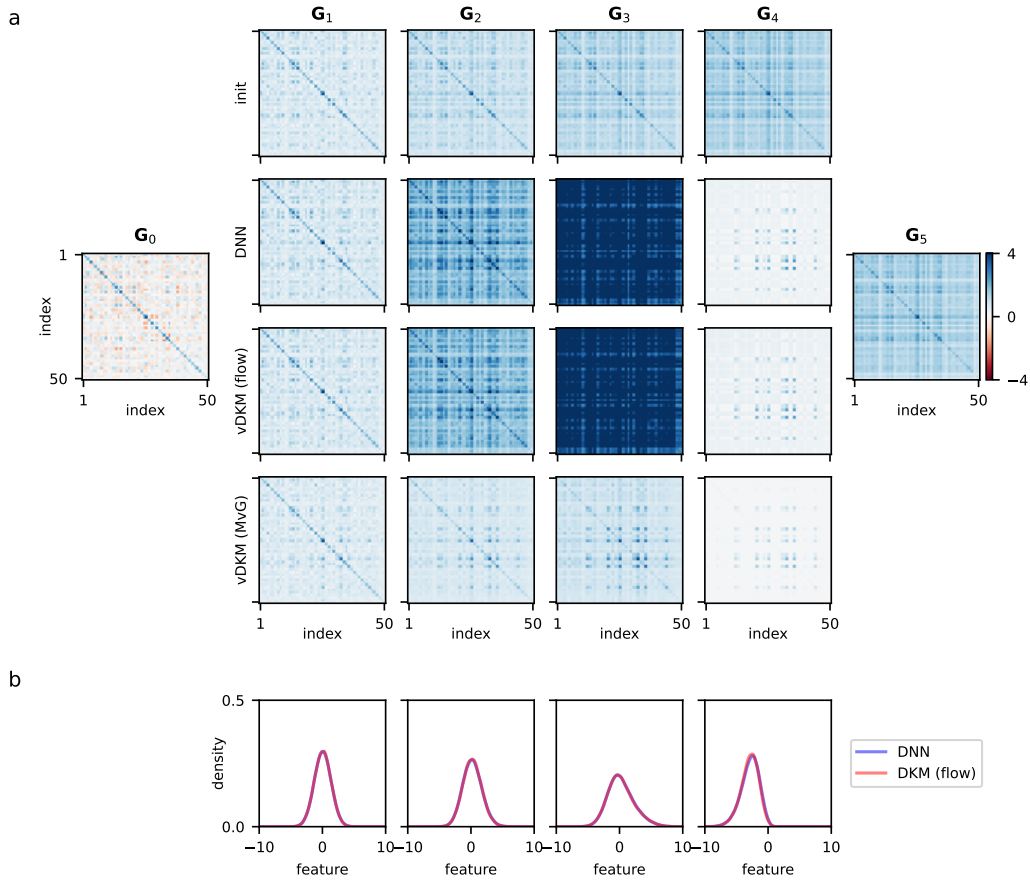


Figure 4: The variational DKM closely matches the DNN true posterior obtained with Langevin sampling. **a** Comparison of Gram matrices. The first two rows show Gram matrices for DNN, with the first row being a random initialization, and the second row being the posterior. The last two rows show the Gram matrices from variational DKMs with a flow approximate posterior (third row) and a multivariate Gaussian approximate posterior (fourth row). In optimizing the variational DKM, we used Eq. (24) with 2^{16} Monte-Carlo samples. The Gram matrices for the flow posterior (third row) closely match those from the DNN posterior (second row). **b** Marginal distributions over features at each layer for one input datapoint estimated using kernel density estimation. The note that the DNN (blue line) marginals are non-Gaussian, but the variational DKM with a flow posterior (red line) is capable of capturing this non-Gaussianity.

Table 2: RMSE for inducing point methods. (Equal) best methods are displayed in bold. Error bars give two stderrs for a paired tests, which uses differences in performance between that method and best method, (so there are no meaningful error bars on the best performing method itself). The MAP objective was numerically unstable and thus did not run to completion on the boston dataset.

| dataset | Kernel Hyper | MAP | \mathcal{L} |
|----------|--------------------------------|--------------------------------|---------------------------------------|
| boston | 4.41 ± 0.31 | — | 4.35 ± 0.51 |
| concrete | 5.38 ± 0.098 | 5.60 ± 0.15 | 5.10 |
| energy | 0.83 ± 0.076 | 0.73 ± 0.049 | 0.47 |
| kin8nm | $(7.3 \pm 0.06) \cdot 10^{-2}$ | $(7.4 \pm 0.05) \cdot 10^{-2}$ | $6.6 \cdot 10^{-2}$ |
| naval | $(6.4 \pm 0.6) \cdot 10^{-4}$ | $(5.4 \pm 0.5) \cdot 10^{-4}$ | $4.6 \cdot 10^{-4}$ |
| yacht | 0.94 ± 0.058 | 1.14 ± 0.077 | 0.58 |
| power | 3.81 ± 0.091 | 3.73 ± 0.14 | 3.58 |
| protein | 4.21 ± 0.029 | 4.30 ± 0.033 | 4.10 |
| wine | 0.68 ± 0.0084 | 0.66 ± 0.0067 | 0.64 |

Inspired by GPs, we designed a scalable inducing point inference method, (Appendix K), and used 300 inducing points fixed to a random subset of the training data and not optimised during training. We used the Adam optimizer with a learning rate of 0.001, full-batch gradients and 5000 iterations for smaller datasets and 1000 iterations for larger datasets (kin8nm, naval and protein).

We found that the deep kernel machine objective gave better performance than MAP, or the hyperparameter optimization baseline (Tab. 2). While these numbers look reasonable compared to those in the deep GP literature [34], they are not directly comparable, as deep GPs are fully Bayesian, while deep kernel machines are not (as they replicate the data infinitely many times), so DKMs cannot offer the same protection against overfitting.

3 Discussion

We introduced the representation learning limit, a new theoretically tractable infinite-width limit for DNNs and DGPs that retains representation learning. Representation learning in this limit is described by the intuitive DKM objective, which is composed of a log-likelihood describing performance on the task (e.g. classification or regression) and a sum of KL-divergences keeping representations at every layer close to those under the prior. For DGPs, the exact posteriors are IID across features and are multivariate Gaussian, with covariances given by optimizing the DKM objective. For DNNs, the exact posteriors are intractable so must be approximated (but as for DGPs, they are IID across features). We found theoretically and empirically that representation learning in DKMs mirrors that in finite-width networks. Finally, we argued that DGPs and DNNs in the representation learning limit form a new class of practical deep kernel method: DKMs. We introduce scalable inducing-point DKMs, and show that the DKM approach performs better than alternatives, including MAP inference on features and standard hyperparameter optimization.

It is important to note that our approach is designed to directly describe the representations in an optimized network, and this focus allowed us to develop the particularly intuitive DKM objective which had potential practical applications e.g. in an inducing-point DKM. There are of course many other theoretical questions in deep learning, including understanding the *dynamics* of representations as networks are trained, e.g. using SGD or Adam [12, 38]. This is necessarily far more complex than our approach of simply characterising the optimum, and thus offers a different type of insight (largely into how to improve neural network training, rather than into the resulting representations themselves e.g. [39]).

There are a number of important directions for future work in the DKM framework. First, at present, we have developed a DKM only for feedforward networks. It will therefore be important to extend scalable DKM approximations to more general network structures, such as convolutional, recurrent [40], graph [41] and transformer networks [42]. Second, we optimized the DKM objective using standard adaptive, gradient-based optimizers such as Adam [43] However, these gradient-based optimizers are designed for very complex and highly multimodal neural network loss landscapes. In contrast, DKM loss landscapes are much simpler and more structured than neural network loss

landscapes, raising the question of whether we can exploit this structure to develop faster optimizers. Finally, the representational perspective offered by the representation learning limit and DKMs may facilitate the development of networks *without* optimization, but which instead initialize each layer in sequence by shaping that layer’s representation towards the top-layer representation [44].

4 Methods

To optimize the analytic DKM objective for DGPs and the variational DKM objective for DGPs (Figs. 2–11), we parameterised the Gram matrices (or covariances for the variational approximate posterior) as the product of a square matrix, $\mathbf{R}_\ell \in \mathbb{R}^{P \times P}$, with itself transposed, $\mathbf{G}_\ell = \frac{1}{P} \mathbf{R}_\ell \mathbf{R}_\ell^T$, and we used Adam with a learning rate of 10^{-3} to learn \mathbf{R}_ℓ . To do Bayesian inference in finite DNNs and DGPs, we used Langevin dynamics with 10 parallel chains, and a step size of 10^{-3} . Note that in certain scenarios, Langevin sampling can be very slow, as the features have a Gaussian prior with covariance $\mathbf{K}(\mathbf{G}_{\ell-1})$ which has some very small and some larger eigenvalues, which makes sampling difficult. Instead, we reparameterised the model in terms of the standard Gaussian random variables, $\mathbf{V}_\ell \in \mathbb{R}^{P \times N_\ell}$. We then wrote \mathbf{F}_ℓ in terms of \mathbf{V}_ℓ ,

$$\mathbf{F}_\ell = \mathbf{L}_{\ell-1} \mathbf{V}_\ell. \quad (28)$$

Here, $\mathbf{L}_{\ell-1}$ is the Cholesky of $\mathbf{K}(\mathbf{G}_{\ell-1})$, so $\mathbf{K}(\mathbf{G}_{\ell-1}) = \mathbf{L}_{\ell-1} \mathbf{L}_{\ell-1}^T$. This gives an equivalent distribution $P(\mathbf{F}_\ell | \mathbf{F}_{\ell-1})$. Importantly, as the prior on \mathbf{V}_ℓ is IID standard Gaussian, sampling \mathbf{V}_ℓ is much faster. To ensure that the computational cost of these expensive simulations remained reasonable, we used a subset of 50 datapoints from each dataset.

For the DKM objective for DNNs, we used Monte-Carlo to approximate the Gram matrices,

$$\mathbf{G}_\theta(\theta_\ell) \approx \sum_{k=1}^K \phi(\mathbf{f}_k^\ell) \phi^T(\mathbf{f}_k^\ell). \quad (29)$$

with \mathbf{f}_k^ℓ drawn from the appropriate approximate posterior, and $K = 2^{16}$. We can use the reparameterisation trick [45, 46] to differentiate through these Monte-Carlo estimates.

References

- [1] Bengio, Y., Courville, A. & Vincent, P. Representation learning: A review and new perspectives. *IEEE transactions on pattern analysis and machine intelligence* **35**, 1798–1828 (2013).
- [2] LeCun, Y., Bengio, Y. & Hinton, G. Deep learning. *nature* **521**, 436–444 (2015).
- [3] Weiss, K., Khoshgoftaar, T. M. & Wang, D. A survey of transfer learning. *Journal of Big data* **3**, 1–40 (2016).
- [4] Neal, R. M. Priors for infinite networks. In *Bayesian Learning for Neural Networks*, 29–53 (Springer, 1996).
- [5] Williams, C. Computing with infinite networks. *Advances in neural information processing systems* **9** (1996).
- [6] Lee, J. *et al.* Deep neural networks as gaussian processes. *arXiv preprint arXiv:1711.00165* (2017).
- [7] Matthews, A. G. d. G., Rowland, M., Hron, J., Turner, R. E. & Ghahramani, Z. Gaussian process behaviour in wide deep neural networks. *arXiv preprint arXiv:1804.11271* (2018).
- [8] Novak, R. *et al.* Bayesian deep convolutional networks with many channels are gaussian processes. *arXiv preprint arXiv:1810.05148* (2018).
- [9] Garriga-Alonso, A., Rasmussen, C. E. & Aitchison, L. Deep convolutional networks as shallow gaussian processes. *arXiv preprint arXiv:1808.05587* (2018).
- [10] Jacot, A., Gabriel, F. & Hongler, C. Neural tangent kernel: Convergence and generalization in neural networks. *Advances in neural information processing systems* **31** (2018).
- [11] Yang, G. Scaling limits of wide neural networks with weight sharing: Gaussian process behavior, gradient independence, and neural tangent kernel derivation. *arXiv preprint arXiv:1902.04760* (2019).

- [12] Yang, G. & Hu, E. J. Feature learning in infinite-width neural networks. *arXiv preprint arXiv:2011.14522* (2020).
- [13] Aitchison, L. Why bigger is not always better: on finite and infinite neural networks. In *International Conference on Machine Learning*, 156–164 (PMLR, 2020).
- [14] Li, Q. & Sompolinsky, H. Statistical mechanics of deep linear neural networks: The back-propagating renormalization group. *arXiv preprint arXiv:2012.04030* (2020).
- [15] Zavatore-Veth, J. A., Canatar, A. & Pehlevan, C. Asymptotics of representation learning in finite bayesian neural networks. *arXiv preprint arXiv:2106.00651* (2021).
- [16] Seroussi, I. & Ringel, Z. Separation of scales and a thermodynamic description of feature learning in some cnns. *arXiv preprint arXiv:2112.15383* (2021).
- [17] Antognini, J. M. Finite size corrections for neural network gaussian processes. *arXiv preprint arXiv:1908.10030* (2019).
- [18] Dyer, E. & Gur-Ari, G. Asymptotics of wide networks from feynman diagrams. *arXiv preprint arXiv:1909.11304* (2019).
- [19] Aitken, K. & Gur-Ari, G. On the asymptotics of wide networks with polynomial activations. *arXiv preprint arXiv:2006.06687* (2020).
- [20] Yaïda, S. Non-gaussian processes and neural networks at finite widths. In *Mathematical and Scientific Machine Learning*, 165–192 (PMLR, 2020).
- [21] Halverson, J., Maiti, A. & Stoner, K. Neural networks and quantum field theory. *Machine Learning: Science and Technology* **2**, 035002 (2021).
- [22] Naveh, G., Ben David, O., Sompolinsky, H. & Ringel, Z. Predicting the outputs of finite deep neural networks trained with noisy gradients. *Phys. Rev. E* **104**, 064301 (2021). URL <https://link.aps.org/doi/10.1103/PhysRevE.104.064301>.
- [23] Zavatore-Veth, J. & Pehlevan, C. Exact marginal prior distributions of finite bayesian neural networks. *Advances in Neural Information Processing Systems* **34** (2021).
- [24] Welling, M. & Teh, Y. W. Bayesian learning via stochastic gradient langevin dynamics. In *Proceedings of the 28th international conference on machine learning (ICML-11)*, 681–688 (Citeseer, 2011).
- [25] Smola, A. J. & Schölkopf, B. *Learning with kernels* (MIT Press, 1998).
- [26] Shawe-Taylor, J. & Cristianini, N. *Kernel methods for pattern analysis* (Cambridge university press, 2004).
- [27] Hofmann, T., Schölkopf, B. & Smola, A. J. Kernel methods in machine learning. *The annals of statistics* 1171–1220 (2008).
- [28] Krizhevsky, A., Sutskever, I. & Hinton, G. E. Imagenet classification with deep convolutional neural networks. *Advances in neural information processing systems* **25** (2012).
- [29] Williams, C. K. & Rasmussen, C. E. *Gaussian processes for machine learning* (MIT press Cambridge, MA, 2006).
- [30] Cho, Y. & Saul, L. K. Kernel methods for deep learning. In *NIPS*, 342–350 (Curran Associates, Inc., 2009).
- [31] Aitchison, L., Yang, A. X. & Ober, S. W. Deep kernel processes. *arXiv preprint arXiv:2010.01590* (2020).
- [32] Jordan, M. I., Ghahramani, Z., Jaakkola, T. S. & Saul, L. K. An introduction to variational methods for graphical models. *Machine learning* **37**, 183–233 (1999).
- [33] Blei, D. M., Kucukelbir, A. & McAuliffe, J. D. Variational inference: A review for statisticians. *Journal of the American statistical Association* **112**, 859–877 (2017).
- [34] Salimbeni, H. & Deisenroth, M. Doubly stochastic variational inference for deep gaussian processes. *arXiv preprint arXiv:1705.08933* (2017).
- [35] Durkan, C., Bekasov, A., Murray, I. & Papamakarios, G. Neural spline flows. *Advances in neural information processing systems* **32** (2019).
- [36] Cai, T. T. & Zhang, L. High-dimensional gaussian copula regression: Adaptive estimation and statistical inference. *Statistica Sinica* 963–993 (2018).

- [37] Gal, Y. & Ghahramani, Z. Dropout as a Bayesian approximation: Representing model uncertainty in deep learning. In *Proceedings of the 33rd International Conference on Machine Learning (ICML-16)* (2016).
- [38] Bordelon, B. & Pehlevan, C. Self-consistent dynamical field theory of kernel evolution in wide neural networks. *arXiv preprint arXiv:2205.09653* (2022).
- [39] Yang, G. *et al.* Tuning large neural networks via zero-shot hyperparameter transfer. *Advances in Neural Information Processing Systems* **34** (2021).
- [40] Hochreiter, S. & Schmidhuber, J. Long short-term memory. *Neural computation* **9**, 1735–1780 (1997).
- [41] Scarselli, F., Gori, M., Tsoi, A. C., Hagenbuchner, M. & Monfardini, G. The graph neural network model. *IEEE transactions on neural networks* **20**, 61–80 (2008).
- [42] Vaswani, A. *et al.* Attention is all you need. *Advances in neural information processing systems* **30** (2017).
- [43] Kingma, D. P. & Ba, J. Adam: A method for stochastic optimization. *arXiv preprint arXiv:1412.6980* (2014).
- [44] Wu, C., Masoomi, A., Gretton, A. & Dy, J. Deep layer-wise networks have closed-form weights. *arXiv preprint arXiv:2202.01210* (2022).
- [45] Kingma, D. P. & Welling, M. Auto-encoding variational bayes. *arXiv preprint arXiv:1312.6114* (2013).
- [46] Rezende, D. J., Mohamed, S. & Wierstra, D. Stochastic backpropagation and approximate inference in deep generative models. In *International conference on machine learning*, 1278–1286 (PMLR, 2014).
- [47] Horn, R. A. & Johnson, C. R. *Matrix analysis* (Cambridge university press, 2012).
- [48] Horn, R. A., Horn, R. A. & Johnson, C. R. *Topics in matrix analysis* (Cambridge university press, 1994).

A General likelihoods that depend only on Gram matrices

We consider very general likelihoods which depend only on the top-layer Gram matrix, \mathbf{G}_L ,

$$P(\mathbf{Y}|\mathbf{G}_L) = \int d\mathbf{F}_{L+1} P(\mathbf{Y}|\mathbf{F}_{L+1}) P(\mathbf{F}_{L+1}|\mathbf{G}_L) \quad (30)$$

where,

$$P(\mathbf{F}_{L+1}|\mathbf{G}_L) = \prod_{\lambda=1}^{N_{L+1}} \mathcal{N}(\mathbf{f}_\lambda^{L+1}; \mathbf{0}, \mathbf{K}(\mathbf{G}_L)). \quad (31)$$

This is a very general class of likelihoods that captures regression,

$$P(\mathbf{y}_\lambda|\mathbf{f}_\lambda^{L+1}) = \mathcal{N}(\mathbf{y}_\lambda^{L+1}; \mathbf{f}_\lambda^{L+1}, \sigma^2 \mathbf{I}), \quad (32)$$

(which is equivalent to the model used in the main text Eq. 1b) and e.g. classification,

$$P(\mathbf{Y}|\mathbf{F}) = \text{categorical}(\mathbf{Y}; \text{softmax}(\mathbf{F}_{L+1})). \quad (33)$$

B Bayesian neural networks fall within our model class

Consider a neural network of the form,

$$\mathbf{F}_1 = \mathbf{X}\mathbf{W}_0 \quad (34a)$$

$$\mathbf{F}_\ell = \phi(\mathbf{F}_{\ell-1})\mathbf{W}_{\ell-1} \quad \text{for } \ell \in \{2, \dots, L+1\} \quad (34b)$$

$$W_{\lambda\mu}^\ell \sim \mathcal{N}\left(0, \frac{1}{N_\ell}\right) \quad W_{\lambda\mu}^0 \sim \mathcal{N}\left(0, \frac{1}{\nu_0}\right) \quad (34c)$$

where $\mathbf{W}_0 \in \mathbb{R}^{\nu_0 \times N_1}$, $\mathbf{W}_\ell \in \mathbb{R}^{N_\ell \times N_{\ell+1}}$ and $\mathbf{W}_{L+1} \in \mathbb{R}^{N_L \times \nu_{L+1}}$ are weight matrices with independent Gaussian priors and ϕ is the usually pointwise nonlinearity.

In principle, we could integrate out the distribution over \mathbf{W}_ℓ to find $P(\mathbf{F}_\ell|\mathbf{F}_{\ell-1})$

$$P(\mathbf{F}_\ell|\mathbf{F}_{\ell-1}) = \int d\mathbf{W}_\ell P(\mathbf{W}_\ell) \delta(\mathbf{F}_\ell - \phi(\mathbf{F}_{\ell-1})\mathbf{W}_\ell), \quad (35)$$

where δ is the Dirac delta. In practice, it is much easier to note that conditioned on $\mathbf{F}_{\ell-1}$, the random variables interest, \mathbf{F}_ℓ are a linear combination of Gaussian distributed random variables, \mathbf{W}_ℓ , and that this Gaussian is completely characterised by its mean and variance. Thus, all we need to do is find the mean and variance of $P(\mathbf{F}_\ell|\mathbf{F}_{\ell-1})$. We begin by writing the feature vectors, \mathbf{f}_λ^ℓ in terms of weight vectors, \mathbf{w}_λ^ℓ ,

$$\mathbf{f}_\lambda^\ell = \phi(\mathbf{F}_{\ell-1})\mathbf{w}_\lambda^\ell. \quad (36)$$

As the prior over weight vectors is IID, the prior over features, conditioned on $\mathbf{F}_{\ell-1}$, is also IID,

$$P(\mathbf{W}) = \prod_{\lambda=1}^{N_\ell} P(\mathbf{w}_\lambda^\ell) = \prod_{\lambda=1}^{N_\ell} \mathcal{N}\left(\mathbf{w}_\lambda^\ell; \mathbf{0}, \frac{1}{N_{\ell-1}} \mathbf{I}\right). \quad (37)$$

$$P(\mathbf{F}_\ell|\mathbf{F}_{\ell-1}) = \prod_{\lambda=1}^{N_\ell} P(\mathbf{f}_\lambda^\ell|\mathbf{F}_{\ell-1}). \quad (38)$$

The mean of \mathbf{f}_λ^ℓ conditioned on $\mathbf{F}_{\ell-1}$ is $\mathbf{0}$,

$$\mathbb{E}[\mathbf{f}_\lambda^\ell|\mathbf{F}_{\ell-1}] = \mathbb{E}[\phi(\mathbf{F}_{\ell-1})\mathbf{w}_\lambda^\ell|\mathbf{F}_{\ell-1}] = \phi(\mathbf{F}_{\ell-1}) \mathbb{E}[\mathbf{w}_\lambda^\ell|\mathbf{F}_{\ell-1}] = \phi(\mathbf{F}_{\ell-1}) \mathbb{E}[\mathbf{w}_\lambda^\ell] = \mathbf{0}. \quad (39)$$

The covariance of \mathbf{f}_λ^ℓ conditioned on $\mathbf{F}_{\ell-1}$ is,

$$\begin{aligned} \mathbb{E}[\mathbf{f}_\lambda^\ell (\mathbf{f}_\lambda^\ell)^T | \mathbf{F}_{\ell-1}] &= \mathbb{E}[\phi(\mathbf{F}_{\ell-1})\mathbf{w}_\lambda^\ell (\phi(\mathbf{F}_{\ell-1})\mathbf{w}_\lambda^\ell)^T | \mathbf{F}_{\ell-1}] \\ &= \phi(\mathbf{F}_{\ell-1}) \mathbb{E}[\mathbf{w}_\lambda^\ell (\mathbf{w}_\lambda^\ell)^T] \phi^T(\mathbf{F}_{\ell-1}) \\ &= \frac{1}{N_{\ell-1}} \phi(\mathbf{F}_{\ell-1}) \phi^T(\mathbf{F}_{\ell-1}) \end{aligned} \quad (40)$$

Thus, the distribution over features is IID Gaussian with zero mean $\mathbf{0}$ and this covariance, as in the main text (Eq. 1a with Eq. 2).

C Weak convergence

Here, we give a formal argument for weak convergence of the DGP posterior over Gram matrices to a point distribution in the limit as $N \rightarrow \infty$,

$$P_N(\mathbf{G}_1, \dots, \mathbf{G}_L | \mathbf{X}, \tilde{\mathbf{Y}}) \xrightarrow{d} \prod_{\ell=1}^L \delta(\mathbf{G}_\ell - \mathbf{G}_\ell^*) \quad (41)$$

where we have included N in the subscript of the probability distribution as a reminder that this distribution depends on the width. By the Portmanteau theorem, weak convergence is established if all expectations of bounded continuous functions, f , converge

$$\lim_{N \rightarrow \infty} \mathbb{E}_{P_N(\mathbf{G}_1, \dots, \mathbf{G}_L | \mathbf{X}, \tilde{\mathbf{Y}})} [f(\mathbf{G}_1, \dots, \mathbf{G}_L)] = f(\mathbf{G}_1^*, \dots, \mathbf{G}_L^*). \quad (42)$$

To show this in a reasonably general setting (which the DGP posterior is a special case of), we consider an unnormalized probability density of the form $h(g)e^{N\mathcal{L}(g)}$, and compute the moment as,

$$\mathbb{E}[f(g)] = \frac{\int_{\mathcal{G}} dg f(g) h(g) e^{N\mathcal{L}(g)}}{\int_{\mathcal{G}} dg h(g) e^{N\mathcal{L}(g)}} \quad (43)$$

where $g = (\mathbf{G}_1, \dots, \mathbf{G}_L)$ is all L positive semi-definite matrices, \mathbf{G}_ℓ . Thus, $g \in \mathcal{G}$, where \mathcal{G} is a convex set.

We consider the superlevel set $A(\Delta) = \{g | \mathcal{L}(g) \geq \mathcal{L}(g^*) - \Delta\}$, where g^* is the unique global optimum. We select out a small region, $A(\Delta)$, surrounding the global maximum, and compute the integral as,

$$\mathbb{E}[f(g)] = \frac{\int_{A(\Delta)} dg f(g) h(g) e^{N\mathcal{L}(g)} + \int_{\mathcal{G} \setminus A(\Delta)} dg f(g) h(g) e^{N\mathcal{L}(g)}}{\int_{A(\Delta)} dg h(g) e^{N\mathcal{L}(g)} + \int_{\mathcal{G} \setminus A(\Delta)} dg h(g) e^{N\mathcal{L}(g)}} \quad (44)$$

And divide the numerator and denominator by $\int_{A(\Delta)} dg h(g) e^{N\mathcal{L}(g)}$,

$$\mathbb{E}[f(g)] = \frac{\frac{\int_{A(\Delta)} dg f(g) h(g) e^{N\mathcal{L}(g)}}{\int_{A(\Delta)} dg h(g) e^{N\mathcal{L}(g)}} + \frac{\int_{\mathcal{G} \setminus A(\Delta)} dg f(g) h(g) e^{N\mathcal{L}(g)}}{\int_{A(\Delta)} dg h(g) e^{N\mathcal{L}(g)}}}{1 + \frac{\int_{\mathcal{G} \setminus A(\Delta)} dg h(g) e^{N\mathcal{L}(g)}}{\int_{A(\Delta)} dg h(g) e^{N\mathcal{L}(g)}}} \quad (45)$$

Now, we deal with each term separately. The ratio in the denominator can be lower-bounded by zero, and upper bounded by considering a smaller superlevel set, $A(\Delta/2)$, in the denominator,

$$\begin{aligned} 0 \leq \frac{\int_{\mathcal{G} \setminus A(\Delta)} dg h(g) e^{N\mathcal{L}(g)}}{\int_{A(\Delta)} dg h(g) e^{N\mathcal{L}(g)}} &\leq \frac{\int_{\mathcal{G} \setminus A(\Delta)} dg h(g) e^{N\mathcal{L}(g)}}{\int_{A(\Delta/2)} dg h(g) e^{N\mathcal{L}(g)}} \\ &\leq \frac{e^{N(\mathcal{L}(g^*) - \Delta)} \int_{\mathcal{G} \setminus A(\Delta)} dg h(g)}{e^{N(\mathcal{L}(g^*) - \Delta/2)} \int_{A(\Delta/2)} dg h(g)} \\ &= \frac{\int_{\mathcal{G} \setminus A(\Delta)} dg h(g)}{\int_{A(\Delta/2)} dg h(g)} e^{-N\Delta/2} \end{aligned} \quad (46)$$

The upper bound converges to zero (as $h(g)$ is independent of N), and therefore by the sandwich theorem the ratio of interest also tends to zero.

The second ratio in the numerator can be rewritten as,

$$\frac{\int_{\mathcal{G} \setminus A(\Delta)} dg f(g) h(g) e^{N\mathcal{L}(g)}}{\int_{A(\Delta)} dg h(g) e^{N\mathcal{L}(g)}} = \frac{\int_{\mathcal{G} \setminus A(\Delta)} dg f(g) h(g) e^{N\mathcal{L}(g)}}{\int_{\mathcal{G} \setminus A(\Delta)} dg h(g) e^{N\mathcal{L}(g)}} \frac{\int_{\mathcal{G} \setminus A(\Delta)} dg h(g) e^{N\mathcal{L}(g)}}{\int_{A(\Delta)} dg h(g) e^{N\mathcal{L}(g)}} \quad (47)$$

The first term here is an expectation of a bounded function, $f(g)$, so is bounded, while second term converges to zero in the limit (by the previous result).

Finally, we consider the first ratio in the numerator,

$$\frac{\int_{A(\Delta)} dg f(g)h(g)e^{N\mathcal{L}(g)}}{\int_{A(\Delta)} dg h(g)e^{N\mathcal{L}(g)}} \quad (48)$$

which can be understood as an expectation over $f(g)$ in the region $A(\Delta)$. As f is continuous, for any $\epsilon > 0$, we can find a $\delta > 0$ such that for all g with $|g^* - g| < \delta$, we have

$$f(g^*) - \epsilon < f(g) < f(g^*) + \epsilon \quad (49)$$

Further, because the continuous function, $\mathcal{L}(g)$, has a unique global optimum, g^* , for every $\delta > 0$ we are always able to find a $\Delta > 0$ such that all points $g \in A(\Delta)$ are within δ of g^* i.e. $|g^* - g| < \delta$. Thus combining the previous two facts, given an ϵ , we are always able to find a δ such that Eq. 49 holds for all g with $|g^* - g| < \delta$, and given a δ we are always able to find a Δ such that all $g \in A(\Delta)$ have $|g^* - g| < \delta$. Hence for every $\epsilon > 0$ we can find a $\Delta > 0$ such that Eq. 49 holds for all $g \in A(\Delta)$. Choosing the appropriate ϵ -dependent Δ and substituting Eq. 49 into Eq. 48, ϵ also bounds the error in the expectation,

$$f(g^*) - \epsilon < \frac{\int_{A(\Delta)} dg f(g)h(g)e^{N\mathcal{L}(g)}}{\int_{A(\Delta)} dg h(g)e^{N\mathcal{L}(g)}} < f(g^*) + \epsilon \quad (50)$$

Now, we use the results in Eq. (46), Eq. (47) and Eq. (50) to take the limit of Eq. (45) (we can compose these limits by the algebraic limit theorem as all the individual limits exist and are finite),

$$f(g^*) - \epsilon < \lim_{N \rightarrow \infty} \mathbb{E}[f(g)] < f(g^*) + \epsilon \quad (51)$$

And as this holds for any ϵ , we have,

$$f(g^*) = \lim_{N \rightarrow \infty} \mathbb{E}[f(g)]. \quad (52)$$

This result is applicable to the DGP posterior over Gram matrices, as that posterior can be written as,

$$P_N(\mathbf{G}_1, \dots, \mathbf{G}_L | \mathbf{X}, \tilde{\mathbf{Y}}) \propto h(g)e^{N\mathcal{L}(g)}. \quad (53)$$

where $\mathcal{L}(g)$ is the usual DKM objective,

$$\mathcal{L}(g) = \mathcal{L}(\mathbf{G}_1, \dots, \mathbf{G}_L). \quad (54)$$

and $h(g)$ is the remaining terms in the log-posterior which do not depend on N ,

$$h(g) = \exp\left(-\frac{P+1}{2} \sum_{\ell} \log |\mathbf{G}_{\ell}|\right). \quad (55)$$

(this requires $P \leq N$ so that \mathbf{G}_{ℓ} is full-rank).

D General models in the representation learning limit

Overall, our goal is to compute the integral in Eq. (7) in the limit as $N \rightarrow \infty$. While the integral is intractable for general models such as BNNs, we can use variational inference to reason about its properties. In particular, we can bound the integral using the ELBO,

$$\log P(\mathbf{G}_{\ell} | \mathbf{G}_{\ell-1}) \geq \text{ELBO}_{\ell} = \mathbb{E}_{Q(\mathbf{F}_{\ell})} [\log P(\mathbf{G}_{\ell} | \mathbf{F}_{\ell}) + \log P(\mathbf{F}_{\ell} | \mathbf{G}_{\ell-1}) - \log Q(\mathbf{F}_{\ell})] \quad (56)$$

Note that $Q(\mathbf{F}_{\ell})$ here is different from $Q_{\theta_{\ell}}(\mathbf{f}_{\lambda}^{\ell})$ in the main text, both because the approximate posterior here, $Q(\mathbf{F}_{\ell})$ is over all features jointly, \mathbf{F}_{ℓ} , whereas the approximate posterior in the main text is only over a single feature, $\mathbf{f}_{\lambda}^{\ell}$, and because in the main text, we chose a specific family of distribution with parameters θ_{ℓ} , while here we leave the approximate posterior, $Q(\mathbf{F}_{\ell})$ completely unconstrained, so that it has the flexibility to capture the true posterior. Indeed, if the optimal approximate posterior is equal to the true posterior, $Q^*(\mathbf{F}_{\ell}) = P(\mathbf{F}_{\ell} | \mathbf{G}_{\ell-1}, \mathbf{G}_{\ell})$, then the corresponding ELBO is tight, so we get $\log P(\mathbf{G}_{\ell} | \mathbf{G}_{\ell-1}) = \text{ELBO}^*$. Our overall strategy is thus to use variational inference to characterise the optimal approximate which is equal to the true posterior $Q^*(\mathbf{F}_{\ell}) = P(\mathbf{F}_{\ell} | \mathbf{G}_{\ell-1}, \mathbf{G}_{\ell})$ and use the corresponding ELBO to obtain $\log P(\mathbf{G}_{\ell} | \mathbf{G}_{\ell-1})$.

D.1 Characterising exact DNN posteriors

Remember that if the approximate posterior family, $Q(\mathbf{F}_\ell)$ is flexible enough to capture the true posterior $P(\mathbf{F}_\ell|\mathbf{G}_{\ell-1}, \mathbf{G}_\ell)$, then the $Q^*(\mathbf{F}_\ell)$ that optimizes the ELBO is indeed the true posterior, and the ELBO is equal to $\log P(\mathbf{G}_\ell|\mathbf{G}_{\ell-1})$ is tight [32, 33]. Thus, we are careful to ensure that our approximate posterior family captures the true posterior, by ensuring that we only impose constraints on $Q(\mathbf{F}_\ell)$ that must hold for the true posterior, $P(\mathbf{F}_\ell|\mathbf{G}_{\ell-1}, \mathbf{G}_\ell)$. In particular, note that the $P(\mathbf{G}_\ell|\mathbf{F}_\ell)$ term (Eq. 6b) constrains the true posterior to give non-zero mass only to \mathbf{F}_ℓ that satisfy $\mathbf{G}_\ell = \frac{1}{N_\ell} \phi(\mathbf{F}_\ell) \phi^T(\mathbf{F}_\ell)$. However, this constraint is difficult to handle in the general case. We therefore consider an alternative, weaker constraint on expectations, which holds for the true posterior (the first equality below) because Eq. (6b) constrains $\mathbf{G}_\ell = \frac{1}{N_\ell} \phi(\mathbf{F}_\ell) \phi^T(\mathbf{F}_\ell)$. We can therefore impose the same constraint on the approximate posterior,

$$\mathbf{G}_\ell = \mathbb{E}_{P(\mathbf{F}_\ell|\mathbf{G}_\ell, \mathbf{G}_{\ell-1})} \left[\frac{1}{N_\ell} \phi(\mathbf{F}_\ell) \phi^T(\mathbf{F}_\ell) \right] = \mathbb{E}_{Q(\mathbf{F}_\ell)} \left[\frac{1}{N_\ell} \phi(\mathbf{F}_\ell) \phi^T(\mathbf{F}_\ell) \right] \quad (57)$$

Now, we can solve for the optimal $Q(\mathbf{F}_\ell)$ with this constraint on the expectation. In particular, the Lagrangian is obtained by taking the ELBO (Eq. 56), dropping the $\log P(\mathbf{G}_\ell|\mathbf{F}_\ell)$ term representing the equality constraint (that $\mathbf{G}_\ell = \frac{1}{N_\ell} \phi(\mathbf{F}_\ell) \phi^T(\mathbf{F}_\ell)$) and including Lagrange multipliers for the expectation constraint, Λ , (Eq. 57) and the constraint that the distribution must normalize to 1, Λ ,

$$\begin{aligned} L = & \int d\mathbf{F}_\ell Q(\mathbf{F}_\ell) (\log P(\mathbf{F}_\ell|\mathbf{G}_{\ell-1}) - \log Q(\mathbf{F}_\ell)) \\ & + \frac{1}{2} \text{Tr} \left(\Lambda \left(\mathbf{G}_\ell - \int d\mathbf{F}_\ell Q(\mathbf{F}_\ell) \phi(\mathbf{F}_\ell) \phi^T(\mathbf{F}_\ell) \right) \right) + \Lambda \left(1 - \int d\mathbf{F}_\ell Q(\mathbf{F}_\ell) \right) \end{aligned} \quad (58)$$

Differentiating wrt $Q(\mathbf{F}_\ell)$, and solving for the optimal approximate posterior, $Q^*(\mathbf{F}_\ell)$,

$$0 = \left. \frac{\partial L}{\partial Q(\mathbf{F}_\ell)} \right|_{Q^*(\mathbf{F}_\ell)} \quad (59)$$

$$0 = (\log P(\mathbf{F}_\ell|\mathbf{G}_{\ell-1}) - \log Q^*(\mathbf{F}_\ell)) - 1 - \frac{1}{2} \text{Tr}(\Lambda \phi(\mathbf{F}_\ell) \phi^T(\mathbf{F}_\ell)) - \Lambda \quad (60)$$

Solving for $\log Q^*(\mathbf{F}_\ell)$,

$$\log Q^*(\mathbf{F}_\ell) = \log P(\mathbf{F}_\ell|\mathbf{G}_{\ell-1}) - \frac{1}{2} \text{Tr}(\Lambda \phi(\mathbf{F}_\ell) \phi^T(\mathbf{F}_\ell)) + \text{const} \quad (61)$$

Using the cyclic property of the trace,

$$\log Q^*(\mathbf{F}_\ell) = \log P(\mathbf{F}_\ell|\mathbf{G}_{\ell-1}) - \frac{1}{2} \text{Tr}(\phi^T(\mathbf{F}_\ell) \Lambda \phi(\mathbf{F}_\ell)) + \text{const} \quad (62)$$

Thus, $\log Q(\mathbf{F}_\ell)$ can be written as a sum over features,

$$\log Q^*(\mathbf{F}_\ell) = \sum_{\lambda=1}^{N_\ell} [\log P(\mathbf{f}_\lambda^\ell|\mathbf{G}_{\ell-1}) - \frac{1}{2} \phi^T(\mathbf{f}_\lambda^\ell) \Lambda \phi(\mathbf{f}_\lambda^\ell)] + \text{const} = \sum_{\lambda=1}^{N_\ell} \log Q(\mathbf{f}_\lambda^\ell) \quad (63)$$

so, the optimal approximate posterior is IID over features,

$$Q^*(\mathbf{F}_\ell) = \prod_{\lambda=1}^{N_\ell} Q^*(\mathbf{f}_\lambda^\ell). \quad (64)$$

Remember that this approximate posterior was only constrained in expectation, and that this constraint held for the true posterior (Eq. 57). Thus, we might think that this optimal approximate posterior would be equal to the true posterior. However, remember that the true posterior had a tighter constraint, that $\mathbf{G}_\ell = \frac{1}{N_\ell} \phi(\mathbf{F}_\ell) \phi^T(\mathbf{F}_\ell)$, while so far we have only imposed a slightly weaker constraint (Eq. 57). We thus need to check that our optimal approximate posterior does indeed satisfy the constraint on the value of \mathbf{G}_ℓ represented by $P(\mathbf{G}_\ell|\mathbf{F}_\ell)$ in the limit as $N_\ell \rightarrow \infty$. This be shown using the law of large numbers, as \mathbf{f}_λ^ℓ are IID under the optimal approximate posterior, and by using Eq. (57) for the final equality,

$$\lim_{N_\ell \rightarrow \infty} \frac{1}{N_\ell} \phi(\mathbf{F}_\ell) \phi^T(\mathbf{F}_\ell) = \lim_{N_\ell \rightarrow \infty} \frac{1}{N_\ell} \sum_{\lambda=1}^{N_\ell} \phi(\mathbf{f}_\lambda^\ell) \phi^T(\mathbf{f}_\lambda^\ell) = \mathbb{E}_{Q(\mathbf{f}_\lambda^\ell)} [\phi(\mathbf{f}_\lambda^\ell) \phi^T(\mathbf{f}_\lambda^\ell)] = \mathbf{G}_\ell. \quad (65)$$

Thus, the optimal approximate posterior does meet the constraint in the limit as $N_\ell \rightarrow \infty$, so in that limit, the true posterior, like the optimal approximate posterior is IID across features,

$$P(\mathbf{F}_\ell|\mathbf{G}_{\ell-1}, \mathbf{G}_\ell) = Q^*(\mathbf{F}_\ell) = \prod_{\lambda=1}^{N_\ell} Q^*(\mathbf{f}_\lambda^\ell) = \prod_{\ell=1}^{N_\ell} P(\mathbf{f}_\lambda^\ell|\mathbf{G}_{\ell-1}, \mathbf{G}_\ell) \quad (66)$$

D.2 Exactly multivariate Gaussian DGP posteriors

For DGPs, we have $\phi(\mathbf{f}_\lambda^\ell) = \mathbf{f}_\lambda^\ell$, so the optimal approximate posterior is Gaussian,

$$\log Q_{\text{DGP}}^*(\mathbf{f}_\lambda^\ell) = \log P_{\text{DGP}}(\mathbf{f}_\lambda^\ell | \mathbf{G}_{\ell-1}) - \frac{1}{2}(\mathbf{f}_\lambda^\ell)^T \mathbf{\Lambda} \mathbf{f}_\lambda^\ell + \text{const} \quad (67)$$

$$= -\frac{1}{2}(\mathbf{f}_\lambda^\ell)^T (\mathbf{\Lambda} + \mathbf{K}^{-1}(\mathbf{G}_{\ell-1})) \mathbf{f}_\lambda^\ell + \text{const} \quad (68)$$

$$= \log \mathcal{N}(\mathbf{f}_\lambda^\ell; \mathbf{0}, (\mathbf{\Lambda} + \mathbf{K}^{-1}(\mathbf{G}_{\ell-1}))^{-1}). \quad (69)$$

As the approximate posterior and true posterior are IID, the constraint in Eq. (57) becomes,

$$\mathbf{G}_\ell = \mathbb{E}_{P_{\text{DGP}}(\mathbf{f}_\lambda^\ell | \mathbf{G}_\ell, \mathbf{G}_{\ell-1})} [\mathbf{f}_\lambda^\ell (\mathbf{f}_\lambda^\ell)^T] = \mathbb{E}_{Q_{\text{DGP}}^*(\mathbf{f}_\lambda^\ell)} [\mathbf{f}_\lambda^\ell (\mathbf{f}_\lambda^\ell)^T] = (\mathbf{\Lambda} + \mathbf{K}^{-1}(\mathbf{G}_{\ell-1}))^{-1}. \quad (70)$$

As the Lagrange multipliers are unconstrained, we can always set them such that this constraint holds. In that case both the optimal approximate posterior and the true posterior become,

$$P_{\text{DGP}}(\mathbf{f}_\lambda^\ell | \mathbf{G}_{\ell-1} \mathbf{G}_\ell) = Q_{\text{DGP}}^*(\mathbf{f}_\lambda^\ell) = \mathcal{N}(\mathbf{f}_\lambda^\ell; \mathbf{0}, \mathbf{G}_\ell), \quad (71)$$

as required.

D.3 Using the factorisation of the true posterior to obtain $\log P(\mathbf{G}_\ell | \mathbf{G}_{\ell-1})$

Now that we have shown that the true posterior, $P(\mathbf{F}_\ell | \mathbf{G}_{\ell-1}, \mathbf{G}_\ell)$ factorises, we can obtain a simple form for $\log P(\mathbf{G}_\ell | \mathbf{G}_{\ell-1})$. In particular, $\log P(\mathbf{G}_\ell | \mathbf{G}_{\ell-1})$ is equal to the ELBO if we use the true posterior in place of the approximate posterior,

$$\log P(\mathbf{G}_\ell | \mathbf{G}_{\ell-1}) = \mathbb{E}_{P(\mathbf{F}_\ell | \mathbf{G}_{\ell-1}, \mathbf{G}_\ell)} \left[\log P(\mathbf{G}_\ell | \mathbf{F}_\ell) + \log \frac{P(\mathbf{F}_\ell | \mathbf{G}_{\ell-1})}{P(\mathbf{F}_\ell | \mathbf{G}_{\ell-1}, \mathbf{G}_\ell)} \right]. \quad (72)$$

In the limit, the constraint represented by $\log P(\mathbf{G}_\ell | \mathbf{F}_\ell)$ is satisfied, so we can include that term in a constant,

$$\log P(\mathbf{G}_\ell | \mathbf{G}_{\ell-1}) = \mathbb{E}_{P(\mathbf{F}_\ell | \mathbf{G}_{\ell-1}, \mathbf{G}_\ell)} \left[\log \frac{P(\mathbf{F}_\ell | \mathbf{G}_{\ell-1})}{P(\mathbf{F}_\ell | \mathbf{G}_{\ell-1}, \mathbf{G}_\ell)} \right] + \text{const} \quad (73)$$

Now, we use the fact that the prior, $P(\mathbf{F}_\ell | \mathbf{G}_{\ell-1})$ and posterior, $P(\mathbf{F}_\ell | \mathbf{G}_{\ell-1}, \mathbf{G}_\ell)$, are IID across features,

$$\log P(\mathbf{G}_\ell | \mathbf{G}_{\ell-1}) = N_\ell \mathbb{E}_{P(\mathbf{f}_\lambda^\ell | \mathbf{G}_{\ell-1}, \mathbf{G}_\ell)} \left[\log \frac{P(\mathbf{f}_\lambda^\ell | \mathbf{G}_{\ell-1})}{P(\mathbf{f}_\lambda^\ell | \mathbf{G}_{\ell-1}, \mathbf{G}_\ell)} \right] + \text{const} \quad (74)$$

and this expectation is a KL-divergence,

$$\log P(\mathbf{G}_\ell | \mathbf{G}_{\ell-1}) = -N_\ell D_{\text{KL}}(P(\mathbf{f}_\lambda^\ell | \mathbf{G}_{\ell-1}, \mathbf{G}_\ell) \| P(\mathbf{f}_\lambda^\ell | \mathbf{G}_{\ell-1})) + \text{const}. \quad (75)$$

which gives Eq. (20) when we combine with Eq. (10) and take the limit as $N \rightarrow \infty$.

D.4 Parametric approximate posteriors

Eq. (66) represents a considerable simplification, as we now need to consider only a single feature, \mathbf{f}_λ^ℓ , rather than the joint distribution over all features, \mathbf{F}_ℓ . However, in the general case, it is still not possible to compute Eq. (66) because the true posterior is still not tractable. Following the true posteriors derived in the previous section, we could chose a parametric approximate posterior that factorises across features,

$$Q_\theta(\mathbf{F}_1, \dots, \mathbf{F}_L) = \prod_{\ell=1}^L \prod_{\lambda=1}^{N_\ell} Q_{\theta_\ell}(\mathbf{f}_\lambda^\ell). \quad (76)$$

Remember that we optimize the approximate posterior parameters, θ , directly, and set the Gram matrices as a function of θ (Eq. 24). Moreover, $\log P(\mathbf{G}_\ell = \mathbf{G}_\theta(\theta_\ell) | \mathbf{G}_{\ell-1})$ is equal to the ELBO with the true posterior, and is larger than the ELBO with an approximate posterior,

$$\log P(\mathbf{G}_\ell = \mathbf{G}_\theta(\theta_\ell) | \mathbf{G}_{\ell-1}) \quad (77)$$

$$= \mathbb{E}_{P(\mathbf{F}_\ell | \mathbf{G}_{\ell-1}, \mathbf{G}_\ell = \mathbf{G}_\theta(\theta_\ell))} \left[\log P(\mathbf{G}_\ell = \mathbf{G}_\theta(\theta_\ell) | \mathbf{F}_\ell) + \log \frac{P(\mathbf{F}_\lambda^\ell | \mathbf{G}_{\ell-1})}{P(\mathbf{F}_\ell | \mathbf{G}_{\ell-1}, \mathbf{G}_\ell = \mathbf{G}_\theta(\theta_\ell))} \right] \quad (78)$$

$$\geq \mathbb{E}_{Q_\theta(\mathbf{F}_\ell)} \left[\log P(\mathbf{G}_\ell = \mathbf{G}_\theta(\theta_\ell) | \mathbf{F}_\ell) + \log \frac{P(\mathbf{F}_\lambda^\ell | \mathbf{G}_{\ell-1})}{Q_{\theta_\ell}(\mathbf{F}_\ell)} \right] \quad (79)$$

Now, we can cancel the $\log P(\mathbf{G}_\ell = \mathbf{G}_\theta(\theta_\ell) | \mathbf{F}_\ell)$ terms, as the constraint holds both under the true posterior, and under the approximate posterior by Eq. (24),

$$\mathbb{E}_{P(\mathbf{F}_\ell | \mathbf{G}_{\ell-1}, \mathbf{G}_\ell = \mathbf{G}_\theta(\theta_\ell))} \left[\log \frac{P(\mathbf{F}_\ell | \mathbf{G}_{\ell-1})}{P(\mathbf{F}_\ell | \mathbf{G}_{\ell-1}, \mathbf{G}_\ell = \mathbf{G}_\theta(\theta_\ell))} \right] \geq \mathbb{E}_{Q_{\theta_\ell}(\mathbf{F}_\ell)} \left[\log \frac{P(\mathbf{F}_\ell | \mathbf{G}_{\ell-1})}{Q_{\theta_\ell}(\mathbf{F}_\ell)} \right] \quad (80)$$

Using the fact that the prior, posterior and approximate posterior are all IID over features, we can write this inequality in terms of distributions over a single feature, \mathbf{f}_λ^ℓ and divide by N_ℓ ,

$$\mathbb{E}_{P(\mathbf{f}_\lambda^\ell | \mathbf{G}_{\ell-1}, \mathbf{G}_\ell = \mathbf{G}_\theta(\theta_\ell))} \left[\log \frac{P(\mathbf{f}_\lambda^\ell | \mathbf{G}_{\ell-1})}{P(\mathbf{f}_\lambda^\ell | \mathbf{G}_{\ell-1}, \mathbf{G}_\ell = \mathbf{G}_\theta(\theta_\ell))} \right] \geq \mathbb{E}_{Q_{\theta_\ell}(\mathbf{f}_\lambda^\ell)} \left[\log \frac{P(\mathbf{f}_\lambda^\ell | \mathbf{G}_{\ell-1}(\theta))}{Q_{\theta_\ell}(\mathbf{f}_\lambda^\ell)} \right]. \quad (81)$$

Noting that both sides of this inequality are negative KL-divergences, we obtain Eq. (23) in the main text.

E Theoretical similarities in representation learning in finite and infinite networks

Here, we consider two arguments. First, we show that MAP inference over features gives the exact same result for any N (finite or infinite). Second, we show that the expected Langevin updates to the Gram matrix are the same, irrespective of N and are equivalent to preconditioned optimization of the DKM objective.

E.1 Equivalence of MAP for DGP features

In the main text, we considered probability densities of the Gram matrices, $\mathbf{G}_1, \dots, \mathbf{G}_L$. However, we can also consider probability densities of the features, $\mathbf{F}_1, \dots, \mathbf{F}_L$, for a DGP,

$$\log P(\mathbf{F}_\ell | \mathbf{F}_{\ell-1}) = -\frac{N_\ell}{2} \log |\mathbf{K}_{\text{DGP}}(\mathbf{G}_{\text{DGP}}(\mathbf{F}_{\ell-1}))| - \frac{1}{2} \text{tr}(\mathbf{F}_\ell^T \mathbf{K}_{\text{DGP}}^{-1}(\mathbf{G}_{\text{DGP}}(\mathbf{F}_{\ell-1})) \mathbf{F}_\ell) + \text{const} \quad (82)$$

We can rewrite the density such that it is still the density of features, \mathbf{F}_ℓ , but it is expressed in terms of the DGP Gram matrix,

$$\log P(\mathbf{F}_\ell | \mathbf{F}_{\ell-1}) = -\frac{N_\ell}{2} \log |\mathbf{K}_{\text{DGP}}(\mathbf{G}_{\ell-1})| - \frac{N_\ell}{2} \text{tr}(\mathbf{K}_{\text{DGP}}^{-1}(\mathbf{G}_{\ell-1}) \mathbf{G}_\ell) + \text{const}. \quad (83)$$

Here, we have used the cyclic property of the trace to combine the \mathbf{F}_ℓ and \mathbf{F}_ℓ^T to form \mathbf{G}_ℓ , and we have used the fact that our kernels can be written as a function of the Gram matrix (Sec. 2.1). Overall, we can therefore write the posterior over features, $P(\mathbf{F}_1, \dots, \mathbf{F}_L | \mathbf{X}, \tilde{\mathbf{Y}})$, in terms of only Gram matrices,

$$\mathcal{J}(\mathbf{G}_1, \dots, \mathbf{G}_L) = \frac{1}{N} P(\mathbf{F}_1, \dots, \mathbf{F}_L | \mathbf{X}, \tilde{\mathbf{Y}}) = \log P(\mathbf{Y} | \mathbf{G}_L) + \frac{1}{N} \sum_{\ell=1}^L \log P(\mathbf{F}_\ell | \mathbf{F}_{\ell-1}), \quad (84)$$

substituting Eq. (83),

$$\mathcal{J}(\mathbf{G}_1, \dots, \mathbf{G}_L) = \log P(\mathbf{Y} | \mathbf{G}_L) - \frac{1}{2} \sum_{\ell=1}^L \nu_\ell (\log |\mathbf{K}_{\text{DGP}}(\mathbf{G}_{\ell-1})| + \text{tr}(\mathbf{K}_{\text{DGP}}^{-1}(\mathbf{G}_{\ell-1}) \mathbf{G}_\ell)) + \text{const}. \quad (85)$$

Thus, $\mathcal{J}(\mathbf{G}_1, \dots, \mathbf{G}_L)$ does not depend on N , and thus the Gram matrices that maximize $\mathcal{J}(\mathbf{G}_1, \dots, \mathbf{G}_L)$ are the same for any choice of N . The only restriction is that we need $N_\ell \geq P$, to ensure that the Gram matrices are full-rank.

To confirm these results, we used Adam with a learning rate of 10^{-3} to optimize full-rank Gram matrices with Eq. (85) and to directly do MAP inference over features using Eq. (82). As expected, as the number of features increased, the Gram matrix from MAP inference over features converged rapidly to that expected using Eq. (85) (Fig. 5).

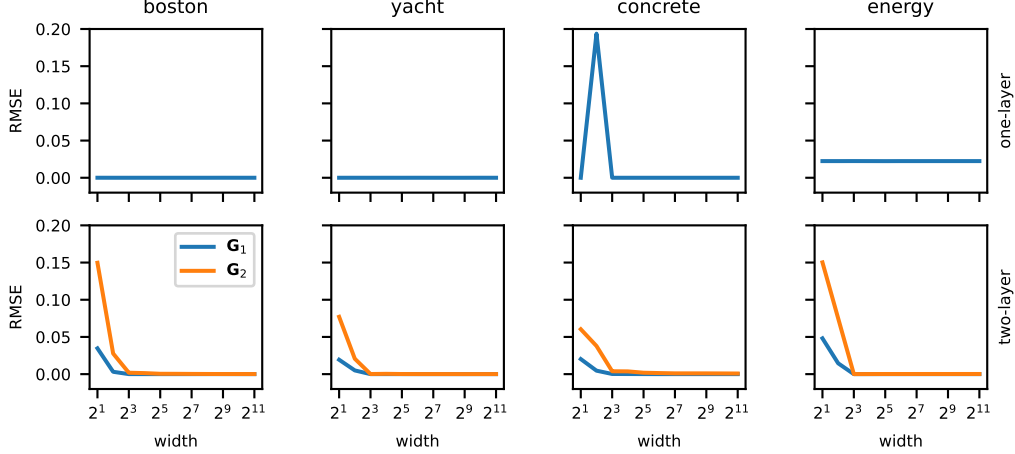


Figure 5: RMSE of trained Gram matrices between one-hidden-layer (first row) and two-hidden-layer (second row) DGPs of various width trained by gradient descent and the corresponding MAP limit. Columns correspond to different datasets (trained on a subset of 50 datapoints).

E.2 Optimizing the deep kernel machine objective for DGPs is equivalent to Langevin sampling

We consider Langevin sampling on the deep Gaussian process model discussed in Sec. 2.1. The deep kernel process paper [31] emphasises that the features at layer ℓ , denoted $\mathbf{F}_\ell \in \mathbb{R}^{P \times N_\ell}$, depend only on the Gram matrix at the previous and next layers, $\mathbf{G}_{\ell-1}$ and $\mathbf{G}_{\ell+1}$, and not on the features at those layers. Now, we consider running Langevin dynamics for \mathbf{F}_ℓ ,

$$d\mathbf{F}_\ell = \frac{1}{2} dt \frac{\partial (N\mathcal{J})}{\partial \mathbf{F}_\ell} + d\Xi, \quad (86)$$

where $d\Xi \in \mathbb{R}^{P \times N_\ell}$ can be understood as IID Gaussian noise (formally, it is the differential of a matrix-valued Wiener process), and $\mathcal{J}(\mathbf{G}_1, \dots, \mathbf{G}_L)$ is the log-joint probability normalized by N (Eq. 84), and where $\mathbf{G}_\ell = \frac{1}{N_\ell} \mathbf{F}_\ell \mathbf{F}_\ell^T$. Thus, the update to \mathbf{G} can be written,

$$\begin{aligned} d\mathbf{G}_\ell &= \frac{1}{N_\ell} d(\mathbf{F}_\ell \mathbf{F}_\ell^T) = \frac{1}{N_\ell} (d\mathbf{F}_\ell \mathbf{F}_\ell^T + \mathbf{F}_\ell d\mathbf{F}_\ell^T + d\mathbf{F}_\ell d\mathbf{F}_\ell^T) \\ &= \frac{1}{2N_\ell} dt \left(\left(\frac{\partial (N\mathcal{J})}{\partial \mathbf{F}_\ell} \right) \mathbf{F}_\ell^T + \mathbf{F}_\ell \left(\frac{\partial (N\mathcal{J})}{\partial \mathbf{F}_\ell} \right)^T \right) + \frac{1}{N_\ell} (d\Xi \mathbf{F}_\ell^T + \mathbf{F}_\ell d\Xi^T) + \frac{1}{N_\ell} d\Xi d\Xi^T. \end{aligned} \quad (88)$$

where the $d\mathbf{F}_\ell d\mathbf{F}_\ell^T$ terms can not be neglected as $d\mathbf{F}_\ell$ contains a Wiener process. Now, we consider all of the stochastic terms, and show that in the infinite width limit, they are deterministic and equal to their expectation. First, we consider $d\Xi d\Xi^T$. Remembering that $\Xi \in \mathbb{R}^{P \times N_\ell}$, the last term can be understood as an average of N_ℓ outer products,

$$\frac{1}{N_\ell} d\Xi d\Xi^T = \frac{1}{N_\ell} \sum_{\lambda=1}^{N_\ell} d\xi_\lambda d\xi_\lambda^T \quad (89)$$

where $\Xi = (\xi_1, \dots, \xi_{N_\ell})$. Taking the limit as the number of intermediate layer features goes to infinity, $N_\ell \rightarrow \infty$, and remembering that ξ_λ are IID for different λ , the law of large numbers tells us that this term becomes deterministic and equal to its expectation,

$$\lim_{N_\ell \rightarrow \infty} \frac{1}{N_\ell} d\Xi d\Xi^T = \mathbb{E} \left[\frac{1}{N_\ell} d\Xi d\Xi^T \right] = \mathbb{E} \left[d\xi_\lambda d\xi_\lambda^T \right] = dt \mathbf{I}, \quad (90)$$

Next, consider an element of $\mathbf{F}_\ell d\Xi$, which is Gaussian, as it is the sum of Gaussian elements in $d\Xi$, which are IID with variance dt ,

$$\frac{1}{N_\ell} \sum_{\lambda=1}^{N_\ell} F_{i\lambda}^\ell d\Xi_{k\lambda} \sim \mathcal{N}(0, dt v_i) \quad (91)$$

Using the definition of the Gram matrix, $\mathbf{G}_\ell = \frac{1}{N_\ell} \mathbf{F}_\ell \mathbf{F}_\ell^T$, the variance is,

$$v_i = \frac{1}{N_\ell^2} \sum_{\lambda=1}^{N_\ell} (F_{i\lambda}^\ell)^2 = \frac{1}{N_\ell} G_{ii}^\ell \quad (92)$$

Thus, the variance goes to zero in the infinite limit,

$$\lim_{N_\ell \rightarrow \infty} v_i = \lim_{N_\ell \rightarrow \infty} \frac{1}{N_\ell} G_{ii}^\ell = 0 \quad \lim_{N_\ell \rightarrow \infty} \frac{1}{N_\ell} \sum_{\lambda=1}^{N_\ell} F_{i\lambda}^\ell d\Xi_{k\lambda} = 0. \quad (93)$$

Thus, in the limit, $\mathbf{F}_\ell d\Xi$ is deterministic and equal to its expected value of 0.

Substituting these results into Eq. (88), and taking the limit $N_\ell \rightarrow \infty$, $d\mathbf{G}_\ell$ becomes deterministic, allowing us to write the dynamics under a Langevin diffusion as,

$$\dot{\mathbf{G}}_\ell = \frac{d\mathbf{G}_\ell}{dt} = \frac{1}{2N_\ell} \left(\left(\frac{\partial(N\mathcal{J})}{\partial \mathbf{F}_\ell} \right) \mathbf{F}_\ell^T + \mathbf{F}_\ell \left(\frac{\partial(N\mathcal{J})}{\partial \mathbf{F}_\ell} \right)^T \right) + \mathbf{I}. \quad (94)$$

Importantly, this is equivalent to the expected $\dot{\mathbf{G}}_\ell$ for finite DGPs, which gives further reason to believe that DKMs will behave similar to finite-width DGPs. Now, our goal is to rewrite this expression entirely in terms of \mathbf{G}_ℓ . As such, we write $\frac{\partial \mathcal{J}}{\partial \mathbf{F}_\ell}$ in terms of $\frac{\partial \mathcal{J}}{\partial \mathbf{G}}$,

$$\frac{\partial \mathcal{J}}{\partial F_{\alpha\beta}^\ell} = \sum_{ij} \frac{\partial \mathcal{J}}{\partial G_{ij}^\ell} \frac{\partial G_{ij}^\ell}{\partial F_{\alpha\beta}^\ell} \quad (95)$$

$$= \frac{1}{N_\ell} \sum_{ij} \frac{\partial \mathcal{J}}{\partial G_{ij}^\ell} \frac{\partial}{\partial F_{\alpha\beta}^\ell} \sum_k F_{ik}^\ell F_{jk}^\ell \quad (96)$$

$$= \frac{1}{N_\ell} \sum_{ij} \frac{\partial \mathcal{J}}{\partial G_{ij}^\ell} \frac{\partial}{\partial F_{\alpha\beta}^\ell} \sum_k (\delta_{\alpha i} \delta_{\beta k} F_{jk}^\ell + F_{ik}^\ell \delta_{\alpha j} \delta_{\beta k}) \quad (97)$$

$$= \frac{1}{N_\ell} \left(\sum_j \frac{\partial \mathcal{J}}{\partial G_{\alpha j}^\ell} F_{j\beta}^\ell + \sum_i \frac{\partial \mathcal{J}}{\partial G_{i\alpha}^\ell} F_{i\beta}^\ell \right), \quad (98)$$

As the gradient of \mathcal{J} wrt \mathbf{G} is symmetric,

$$\frac{\partial(N\mathcal{J})}{\partial \mathbf{F}_\ell} = \frac{2}{N_\ell} \frac{\partial(N\mathcal{J})}{\partial \mathbf{G}} \mathbf{F}_\ell. \quad (99)$$

Thus, we can rewrite the expected updates for \mathbf{G}_ℓ entirely in terms of \mathbf{G}_ℓ and not in terms of \mathbf{F}_ℓ ,

$$\dot{\mathbf{G}}_\ell = \frac{1}{N_\ell^2} \left(\frac{\partial(N\mathcal{J})}{\partial \mathbf{G}_\ell} \mathbf{F}_\ell \mathbf{F}_\ell^T + \mathbf{F}_\ell \mathbf{F}_\ell^T \frac{\partial(N\mathcal{J})}{\partial \mathbf{G}_\ell} \right) + \mathbf{I} \quad (100)$$

using $N_\ell = N\nu_\ell$ and the definition of the Gram matrix, $\mathbf{G}_\ell = \frac{1}{N_\ell} \mathbf{F}_\ell \mathbf{F}_\ell^T$

$$\dot{\mathbf{G}}_\ell = \frac{1}{\nu_\ell} \left(\frac{\partial \mathcal{J}}{\partial \mathbf{G}_\ell} \mathbf{G}_\ell + \mathbf{G}_\ell \frac{\partial \mathcal{J}}{\partial \mathbf{G}_\ell} \right) + \mathbf{I}. \quad (101)$$

Now, we seek to interpret these expected Langevin dynamics as preconditioned gradient descent under a modified loss. Remembering that \mathbf{G}_ℓ is full rank as we have sent $N_\ell \rightarrow \infty$, it makes sense to consider the DKM objective (Eq. 17), which is the log-joint, modified by the inclusion of log-determinant terms,

$$\mathcal{L} = \mathcal{J} + \sum_{\ell=1}^L \frac{\nu_\ell}{2} \log |\mathbf{G}_\ell|. \quad (102)$$

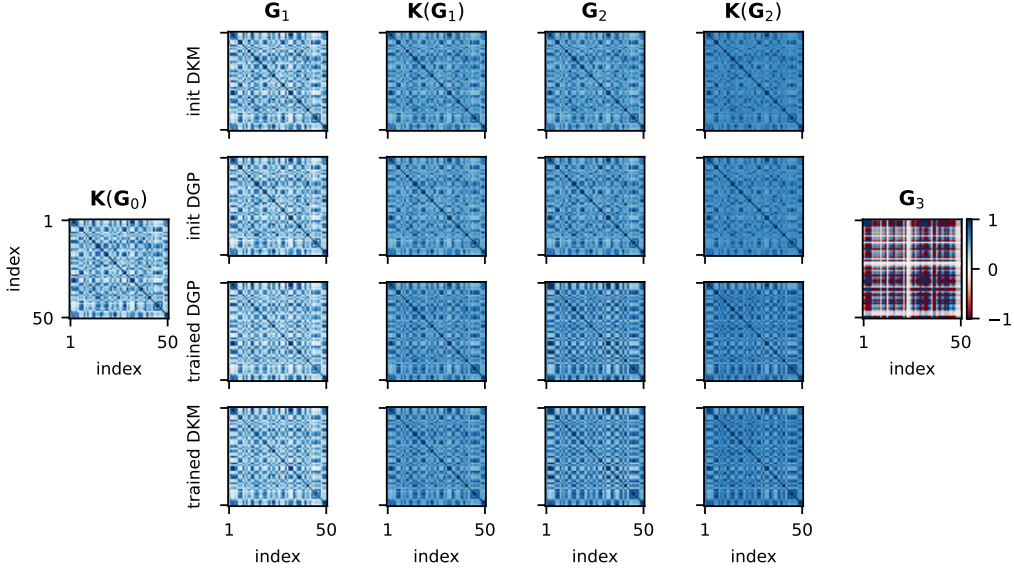


Figure 6: One hidden layer DGP and DKM with squared exponential kernel trained on a subset of energy. First and second row: initializations of DGP and DKM. Third and fourth row: trained DGP (by Langevin dynamics) and DKM Gram matrices and kernels.

Gradients under this objective are,

$$\frac{\partial \mathcal{L}}{\partial \mathbf{G}_\ell} = \frac{\partial \mathcal{J}}{\partial \mathbf{G}_\ell} + \frac{\nu_\ell}{2} \mathbf{G}_\ell^{-1}. \quad (103)$$

We then precondition using the positive definite matrix, $\frac{1}{\nu_\ell} (\mathbf{G}_\ell \otimes \mathbf{I} + \mathbf{I} \otimes \mathbf{G}_\ell)$, where \otimes is the Kronecker product, and $\text{vec}(\cdot)$ takes all elements of a matrix, and rearranges them to form a vector,

$$\frac{1}{\nu_\ell} (\mathbf{G}_\ell \otimes \mathbf{I} + \mathbf{I} \otimes \mathbf{G}_\ell) \text{vec} \left(\frac{\partial \mathcal{L}}{\partial \mathbf{G}_\ell} \right) = (\mathbf{G}_\ell \otimes \mathbf{I} + \mathbf{I} \otimes \mathbf{G}_\ell) \text{vec} \left(\frac{1}{\nu_\ell} \frac{\partial \mathcal{J}}{\partial \mathbf{G}_\ell} + \frac{1}{2} \mathbf{G}_\ell^{-1} \right) \quad (104)$$

$$= \text{vec} \left(\frac{1}{\nu_\ell} \left(\frac{\partial \mathcal{J}}{\partial \mathbf{G}_\ell} \mathbf{G}_\ell + \mathbf{G}_\ell \frac{\partial \mathcal{J}}{\partial \mathbf{G}_\ell} \right) + \mathbf{I} \right). \quad (105)$$

This expression matches the dynamics under Langevin sampling (Eq. 101), so preconditioned gradient descent on \mathcal{L} (Eq. 102) is equivalent to the dynamics on \mathbf{G}_ℓ induced by a Langevin diffusion.

F Additional comparisons with finite-width DGPs

Here, we give additional results supporting those in Sec. 2.7, Fig. 2–Fig. 11. In particular, we give the DGP representations learned by two-layer networks on all UCI datasets (boston, concrete, energy, yacht), except those already given in the main text Fig. 6–8.

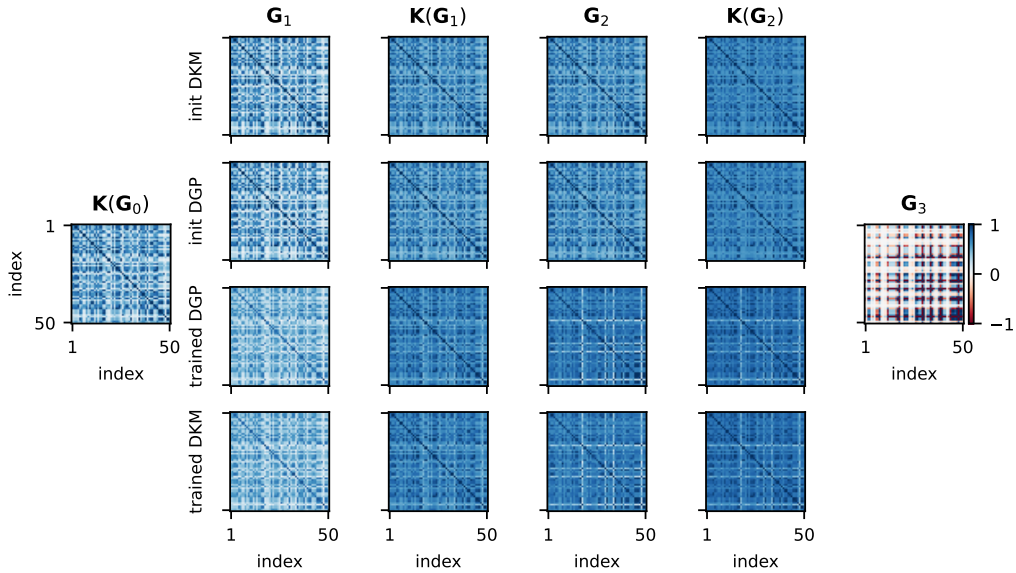


Figure 7: One hidden layer DGP and DKM with squared exponential kernel trained on a subset of boston. First and second row: initializations of DGP and DKM. Third and fourth row: trained DGP (by Langevin dynamics) and DKM Gram matrices and kernels.

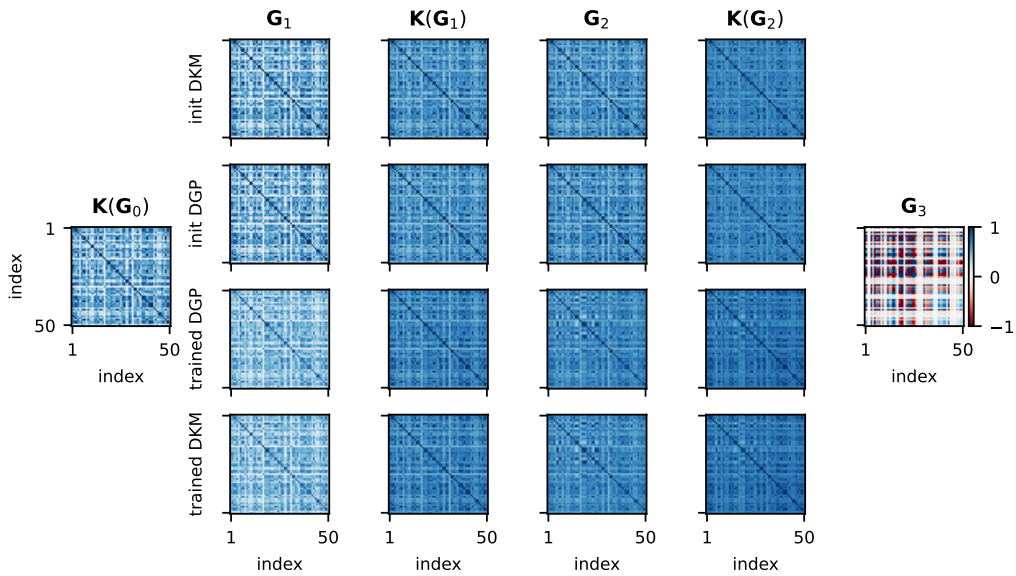


Figure 8: One hidden layer DGP and DKM with squared exponential kernel trained on a subset of concrete. First and second row: initializations of DGP and DKM. Third and fourth row: trained DGP (by Langevin dynamics) and DKM Gram matrices and kernels.

G The flow posterior in a 2-layer DNN

Here, we give the 2-layer version (Fig. 9) of Fig. 4 in the main text, which again shows a close match between the variational DKM with a flow posterior, and the DNN true posterior.

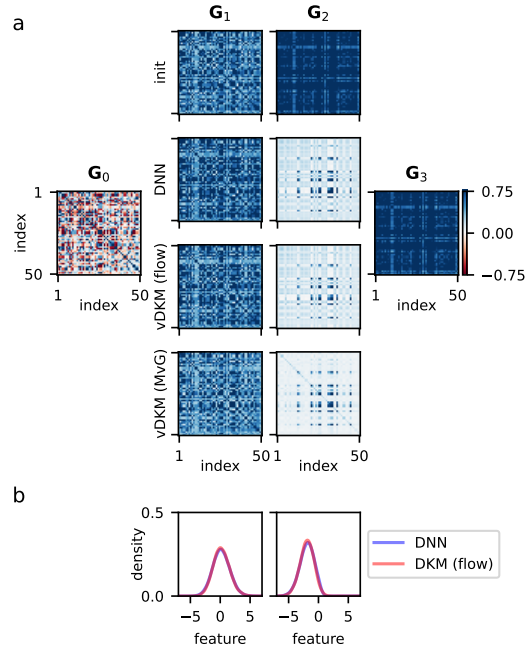


Figure 9: Two-layer ReLU DNN and variational DKM with flow. **a** Initialized (first row) and learned Gram matrices of a width 1024 DNN (second row), vDKM with flow (third row) and vDKM with multivariate Gaussian (fourth row) using 2^{14} Monte-Carlo samples. The Gram matrices between DNN and vDKM (flow) match closely after training. (MvG). **b** Marginal PDF over features at each layer for one input datapoint using kernel density estimation. The marginal PDFs of DNN are non-Gaussian (blue curves), vDKM with flow is able to capture the non-Gaussianity and match closely with DNNs marginals (red curves).

H Multivariate Gaussian approximate posteriors in deeper networks

There is a body of theoretical work (e.g. [16]), on DNNs that approximates DNN posteriors over features as Gaussian. While we have shown that this is a bad idea in general (Fig. 4 and 9), we can nonetheless ask whether there are circumstances where the idea might work well. In particular, we hypothesised that depth is an important factor. In particular, in shallow networks, in order to get \mathbf{G}_L close to the required representation, we may need the posterior over \mathbf{F}_ℓ to be quite different from the prior. In contrast, in deeper networks, we might expect the posterior over \mathbf{F}_ℓ to be closer to its (Gaussian) prior, and therefore we might Gaussian approximate posteriors to work better.

However, we cannot just make the network deeper, because as we do so, we apply the nonlinearity more times and dramatically alter the network’s inductive biases. To resolve this issue, we derive a leaky relu nonlinearity that allows (approximately) independent control over the inductive biases (or effective depth) and the actual depth (Appendix H.1). Using these nonlinearities, we indeed find that very deep networks are reasonably well approximated by multivariate Gaussian approximate posteriors (Appendix H.2).

H.1 Leaky relu nonlinearities

Our goal is to find a pointwise nonlinearity, ϕ , such that (under the prior),

$$\mathbb{E}_{\text{P}_{\text{DGP}}(\mathbf{f}_\lambda^\ell | \mathbf{G}_{\ell-1})} [\phi(\mathbf{f}_\lambda^\ell) \phi^T(\mathbf{f}_\lambda^\ell)] = p \mathbb{E}_{\text{P}(\mathbf{f}_\lambda^\ell | \mathbf{G}_{\ell-1})} [\text{relu}(\mathbf{f}_\lambda^\ell) \text{relu}^T(\mathbf{f}_\lambda^\ell)] + (1-p) \mathbf{G}_{\ell-1}. \quad (106)$$

We will set $p = \alpha/L$, where α is the “effective” depth of the network and L is the real depth. These networks are designed such that their inductive biases in the infinite width limit are similar to a standard relu network with depth α . Indeed, we would take this approach if we wanted a well-defined infinite-depth DKM limit.

Without loss of generality, we consider a 2D case, where x and y are zero-mean bivariate Gaussian,

$$\pi(x, y) = \mathcal{N} \left(\begin{pmatrix} x \\ y \end{pmatrix}; \mathbf{0}, \begin{pmatrix} \Sigma_{xx} & \Sigma_{xy} \\ \Sigma_{xy} & \Sigma_{yy} \end{pmatrix} \right) \quad (107)$$

where $\pi(x, y)$ is the probability density for the joint distribution. Note that we use a scaled relu,

$$\text{relu}(x) = \begin{cases} \sqrt{2} x & \text{for } 0 < x \\ 0 & \text{otherwise} \end{cases} \quad (108)$$

such that $\mathbb{E}[\text{relu}^2(x)] = \Sigma_{xx}$. Mirroring Eq. 106, we want the nonlinearity, ϕ , to satisfy,

$$\mathbb{E}[\phi(x^2)] = p \mathbb{E}[\text{relu}^2(x)] + (1-p) \Sigma_{xx} = \Sigma_{xx} \quad (109a)$$

$$\mathbb{E}[\phi(y^2)] = p \mathbb{E}[\text{relu}^2(y)] + (1-p) \Sigma_{yy} = \Sigma_{yy} \quad (109b)$$

$$\mathbb{E}[\phi(x)\phi(y)] = p \mathbb{E}[\text{relu}(x)\text{relu}(y)] + (1-p) \Sigma_{xy} \quad (109c)$$

We hypothesise that this nonlinearity has the form,

$$\phi(x) = a \text{relu}(x) + bx \quad (110)$$

We will write the relu as a sum of x and $|x|$,

$$\text{relu}(x) = \frac{1}{\sqrt{2}}(x + |x|), \quad (111)$$

because $\mathbb{E}[f(x, y)] = 0$ for $f(x, y) = x|y|$ or $f(x, y) = |x|y$. It turns out that we get zero expectation for all functions where $f(-x, -y) = -f(x, y)$, which holds for the two choices above. To show such functions have a zero expectation, we write out the integral explicitly,

$$\mathbb{E}[f(x, y)] = \int_{-\infty}^{\infty} dx \int_{-\infty}^{\infty} dy \pi(x, y) f(x, y) \quad (112)$$

We split the domain of integration for y at zero,

$$\mathbb{E}[f(x, y)] = \int_{-\infty}^{\infty} dx \int_{-\infty}^0 dy \pi(x, y) f(x, y) + \int_{-\infty}^{\infty} dx \int_0^{\infty} dy \pi(x, y) f(x, y). \quad (113)$$

We substitute $y' = -y$ and $x' = -x$ in the first integral,

$$\mathbb{E}[f(x, y)] = \int_{-\infty}^{\infty} dx' \int_0^{\infty} dy' \pi(-x', -y') f(-x', -y') + \int_{-\infty}^{\infty} dx \int_0^{\infty} dy \pi(x, y) f(x, y). \quad (114)$$

As the variables we integrate over are arbitrary we can relabel y' as y and x' as x , and we can then merge the integrals as their limits are the same,

$$\mathbb{E}[f(x, y)] = \int_{-\infty}^{\infty} dx \int_0^{\infty} dy [\pi(-x, -y) f(-x, -y) + \pi(x, y) f(x, y)] \quad (115)$$

Under a zero-mean Gaussian, $\pi(-x, -y) = \pi(x, y)$,

$$\mathbb{E}[f(x, y)] = \int_{-\infty}^{\infty} dx \int_0^{\infty} dy \pi(x, y) (f(-x, -y) + f(x, y)). \quad (116)$$

Thus, if $f(-x, -y) = -f(x, y)$, then the expectation of that function under a bivariate zero-mean Gaussian distribution is zero.

Remember that our overall goal was to design a nonlinearity, ϕ , (Eq. 110) which satisfied Eq. (109). We therefore compute the expectation,

$$\mathbb{E}[\phi(x)\phi(y)] = \mathbb{E}[(a \operatorname{relu}(x) + bx)(a \operatorname{relu}(y) + by)] \quad (117)$$

$$= \mathbb{E}\left[\left(\frac{a}{\sqrt{2}}(x + |x|) + bx\right)\left(\frac{a}{\sqrt{2}}(y + |y|) + by\right)\right] \quad (118)$$

Using the fact that $\mathbb{E}[x|y|] = \mathbb{E}[|x|y] = 0$ under a multivariate Gaussian,

$$= \mathbb{E}\left[a^2 \frac{1}{\sqrt{2}}(x + |x|) \frac{1}{\sqrt{2}}(y + |y|) + (\sqrt{2}ab + b^2)xy\right] \quad (119)$$

$$= a^2 \mathbb{E}[\operatorname{relu}(x)\operatorname{relu}(y)] + (\sqrt{2}ab + b^2) \mathbb{E}[xy]. \quad (120)$$

Thus, we can find the value of a by comparing with Eq. (109c),

$$p = a^2 \qquad a = \sqrt{p}. \quad (121)$$

For b , things are a bit more involved,

$$1 - p = \sqrt{2}ab + b^2 = \sqrt{2p}b + b^2 \quad (122)$$

where we substitute for the value of a . This can be rearranged to form a quadratic equation in b ,

$$0 = b^2 + \sqrt{2p}b + (p - 1), \quad (123)$$

which can be solved,

$$b = \frac{1}{2} \left(-\sqrt{2p} \pm \sqrt{2p - 4(p - 1)} \right) \quad (124)$$

$$b = \frac{1}{2} \left(-\sqrt{2p} \pm \sqrt{4 - 2p} \right) \quad (125)$$

$$b = -\sqrt{\frac{p}{2}} \pm \sqrt{1 - \frac{p}{2}} \quad (126)$$

Only the positive root is of interest,

$$b = \sqrt{1 - \frac{p}{2}} - \sqrt{\frac{p}{2}} \quad (127)$$

Thus, the nonlinearity is,

$$\phi(x) = \sqrt{p} \operatorname{relu}(x) + \left(\sqrt{1 - \frac{p}{2}} - \sqrt{\frac{p}{2}} \right) x \quad (128)$$

where we set $p = \alpha/L$, and remember we used the scaled relu in Eq. (108). Finally, we established these choices by considering only the cross term, $\mathbb{E}[\phi(x)\phi(y)]$. We also need to check that the $\mathbb{E}[\phi^2(x)]$ and $\mathbb{E}[\phi^2(y)]$ terms are as required (Eq. 109a and Eq. 109b). In particular,

$$\mathbb{E}[\phi^2(x)] = \mathbb{E}[(a \operatorname{relu}(x) + bx)^2] = \mathbb{E}\left[\left(\frac{a}{\sqrt{2}}(x + |x|) + bx\right)^2\right] \quad (129)$$

using $\mathbb{E}[x|x|] = 0$ as $x|x|$ is an odd function of x , and the zero-mean Gaussian is an even distribution,

$$\mathbb{E}[\phi^2(x)] = a^2 \mathbb{E}[\operatorname{relu}^2(x)] + (\sqrt{2}ab + b^2) \Sigma_{xx} \quad (130)$$

using Eq. (121) to identify a^2 and Eq. (122) to identify $\sqrt{2}ab + b^2$,

$$\mathbb{E}[\phi^2(x)] = p \mathbb{E}[\operatorname{relu}^2(x)] + (1 - p) \Sigma_{xx}, \quad (131)$$

as required.

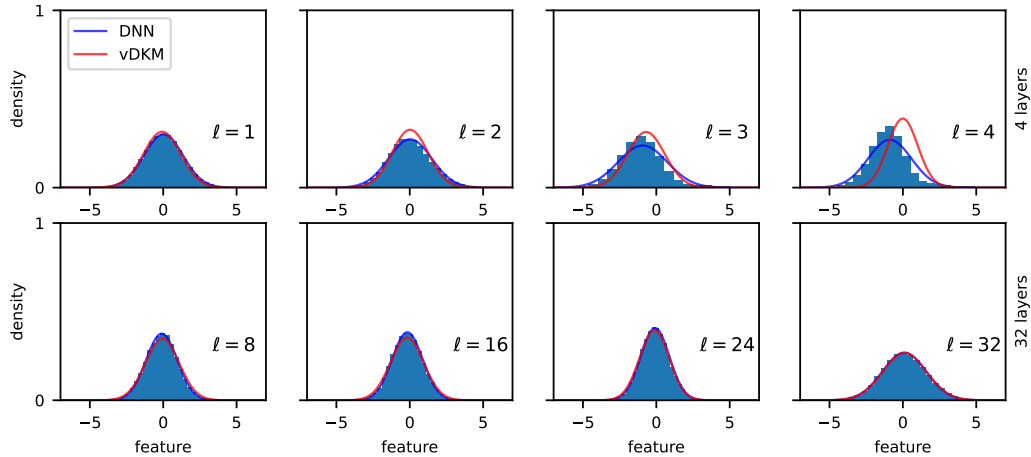


Figure 10: Comparison of posterior feature marginal distributions between a DNN of width 1024 (trained by Langevin sampling over features) and a variational DKM with 2^{16} Monte-Carlo samples, in a 4-layer (row 1) and a 32-layer (row 2) network. We give the DNN posterior features from Langevin sampling (blue histogram) and the best fitting Gaussian (blue line), and compare against the variational DKM approximate posterior Gaussian distribution (red line).

H.2 Multivariate Gaussian in deeper networks

In the main text, we show that a more complex approximate posterior can match the distributions in these networks. Here, we consider an alternative approach. In particular, we hypothesise that these distributions are strongly non-Gaussian because the networks are shallow, meaning that the posterior needs to be far from the prior in order to get a top-layer kernel close to \mathbf{G}_{L+1} . We could therefore make the posteriors closer to Gaussian by using leaky-relu nonlinearities (Appendix H.1) with fixed effective depth ($\alpha = 2$), but increasing real depth, L . In particular, we use multivariate Gaussian approximate posteriors with learned means,

$$Q_{\theta_\ell}(\mathbf{f}_\lambda^\ell) = \mathcal{N}(\mathbf{f}_\lambda^\ell; \boldsymbol{\mu}_\ell, \boldsymbol{\Sigma}_\ell) \quad \text{so} \quad \theta_\ell = (\boldsymbol{\mu}_\ell, \boldsymbol{\Sigma}_\ell). \quad (132)$$

As expected, for a depth 32 network, we have much more similar marginals (Fig. 10 top) and learned representations (Fig. 11 top).

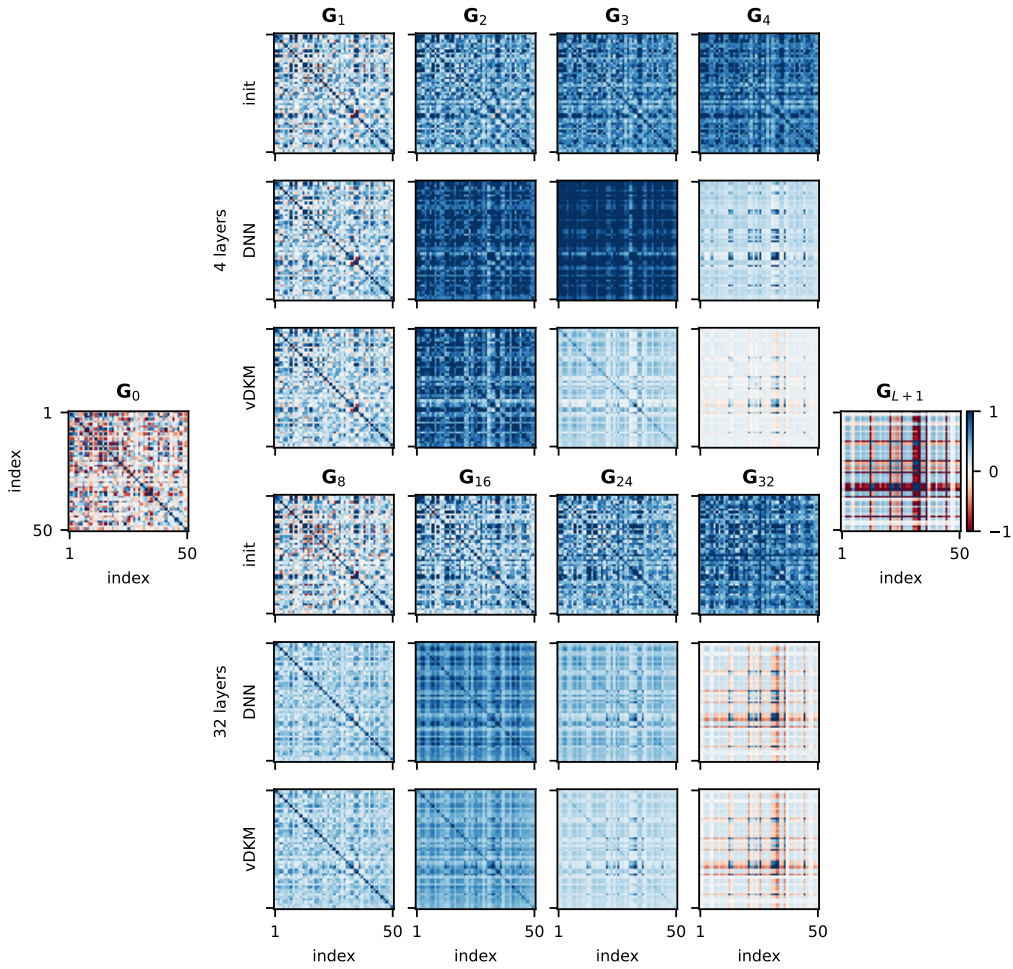


Figure 11: Comparison of Gram matrices between DNN of width 1024 (trained by Langevin sampling over features) and variational DKM, in 4-layer (row 1-3) and 32-layer networks (row 4-6). Initializations are shown in row 1 and 4, trained DNN Gram matrices are shown in row 2 and 5, and trained variational DKM Gram matrices are shown in row 3 and 6. As in Figure 10, the variational DKM is a poor match to Langevin sampling in a DNN for a 4-layer network, but is very similar in a 32 layer network.

I Unimodality in linear deep kernel machines

I.1 Theory: unimodality with a linear kernel and same widths

Here, we show that the deep kernel machine objective is unimodal for a linear kernel. A linear kernel simply returns the input Gram matrix,

$$\mathbf{K}(\mathbf{G}) = \mathbf{G}. \quad (133)$$

It is called a linear kernel, because it arises in the neural network setting (Eq. 34) by choosing the nonlinearity, ϕ to be the identity, in which case, $\mathbf{F}_\ell = \mathbf{F}_{\ell-1} \mathbf{W}_{\ell-1}$. For a linear kernel the objective becomes,

$$\mathcal{L}(\mathbf{G}_1, \dots, \mathbf{G}_L) = \sum_{\ell=1}^{L+1} \frac{\nu_\ell}{2} (\log |\mathbf{G}_{\ell-1}^{-1} \mathbf{G}_\ell| - \text{Tr}(\mathbf{G}_{\ell-1}^{-1} \mathbf{G}_\ell)) \quad (134)$$

where we have assumed there is no output noise, $\sigma^2 = 0$. Taking all ν_ℓ to be equal, $\nu = \nu_\ell$ (see Appendix I.2 for the general case),

$$\mathcal{L}(\mathbf{G}_1, \dots, \mathbf{G}_L) = \log |\mathbf{G}_0^{-1} \mathbf{G}_{L+1}| - \frac{\nu}{2} \sum_{\ell=1}^{L+1} \text{Tr}(\mathbf{G}_{\ell-1}^{-1} \mathbf{G}_\ell). \quad (135)$$

Note that \mathbf{G}_0 and \mathbf{G}_{L+1} are fixed by the inputs and outputs respectively. Thus, to find the mode, we set the gradient wrt $\mathbf{G}_1, \dots, \mathbf{G}_L$ to zero,

$$\mathbf{0} = \frac{\partial \mathcal{L}}{\partial \mathbf{G}_\ell} = \frac{\nu}{2} (\mathbf{G}_{\ell-1}^{-1} - \mathbf{G}_\ell^{-1} \mathbf{G}_{\ell+1} \mathbf{G}_\ell^{-1}) \quad (136)$$

Thus, at the mode, the recursive relationship must hold,

$$\mathbf{T} = \mathbf{G}_{\ell-1}^{-1} \mathbf{G}_\ell = \mathbf{G}_\ell^{-1} \mathbf{G}_{\ell+1}. \quad (137)$$

Thus, optimal Gram matrices are given by,

$$\mathbf{G}_\ell = \mathbf{G}_0 \mathbf{T}^\ell, \quad (138)$$

and we can solve for \mathbf{T} by noting,

$$\mathbf{G}_0^{-1} \mathbf{G}_{L+1} = \mathbf{T}^{L+1}. \quad (139)$$

Importantly, \mathbf{T} is the product of two positive definite matrices, $\mathbf{T} = \mathbf{G}_{\ell-1}^{-1} \mathbf{G}_\ell$, so \mathbf{T} must have positive, real eigenvalues (but \mathbf{T} does not have to be symmetric [47]). There is only one solution to Eq. (139) with positive real eigenvalues [48]. Intuitively, this can be seen using the eigendecomposition, $\mathbf{G}_0^{-1} \mathbf{G}_{L+1} = \mathbf{V}^{-1} \mathbf{D} \mathbf{V}$, where \mathbf{D} is diagonal,

$$\mathbf{T} = (\mathbf{V}^{-1} \mathbf{D} \mathbf{V})^{1/(L+1)} = \mathbf{V}^{-1} \mathbf{D}^{1/(L+1)} \mathbf{V}. \quad (140)$$

Thus, finding \mathbf{T} reduces to finding the $(L+1)$ th root of each positive real number on the diagonal of \mathbf{D} . While there are $(L+1)$ complex roots, there is only one positive real root, and so \mathbf{T} and hence $\mathbf{G}_1, \dots, \mathbf{G}_L$ are uniquely specified. This contrasts with a deep linear neural network, which has infinitely many optimal settings for the weights.

Note that for the objective to be well-defined, we need $\mathbf{K}(\mathbf{G})$ to be full-rank. With standard kernels (such as the squared exponential) this is always the case, even if the input Gram matrix is singular. However, a linear kernel will have a singular output if given a singular input, and with enough data points, $\mathbf{G}_0 = \frac{1}{\nu_0} \mathbf{X} \mathbf{X}^T$ is always singular. To fix this, we could e.g. define $\mathbf{G}_0 = \mathbf{K}(\frac{1}{\nu_0} \mathbf{X} \mathbf{X}^T)$ to be given by applying a positive definite kernel (such as a squared exponential) to $\frac{1}{\nu_0} \mathbf{X} \mathbf{X}^T$. This results in positive definite \mathbf{G}_0 , as long as the input points are distinct.

I.2 Theory: unimodality with a linear kernel and arbitrary widths

In the main text we showed that the deep kernel machine is unimodal when all ν_ℓ are equal. Here, we show that unimodality in linear DKMs also holds for all choices of ν_ℓ . Recall the linear DKM objective in Eq. (134),

$$\mathcal{L}(\mathbf{G}_1, \dots, \mathbf{G}_L) = \sum_{\ell=1}^{L+1} \frac{\nu_\ell}{2} (\log |\mathbf{G}_{\ell-1}^{-1} \mathbf{G}_\ell| - \text{Tr}(\mathbf{G}_{\ell-1}^{-1} \mathbf{G}_\ell)) \quad (141)$$

$$= \sum_{\ell=1}^{L+1} \frac{\nu_\ell}{2} (\log |\mathbf{G}_\ell| - \log |\mathbf{G}_{\ell-1}| - \text{Tr}(\mathbf{G}_{\ell-1}^{-1} \mathbf{G}_\ell)). \quad (142)$$

To find the mode, again we set the gradient wrt \mathbf{G}_ℓ to zero,

$$\mathbf{0} = \frac{\partial \mathcal{L}}{\partial \mathbf{G}_\ell} = -\frac{\nu_{\ell+1} - \nu_\ell}{2} \mathbf{G}_\ell^{-1} - \frac{\nu_\ell}{2} \mathbf{G}_{\ell-1}^{-1} + \frac{\nu_{\ell+1}}{2} \mathbf{G}_\ell^{-1} \mathbf{G}_{\ell+1} \mathbf{G}_\ell^{-1}, \quad (143)$$

for $\ell = 1, \dots, L$. Right multiplying by $2\mathbf{G}_\ell$ and rearranging,

$$\nu_{\ell+1} \mathbf{G}_\ell^{-1} \mathbf{G}_{\ell+1} = \nu_\ell \mathbf{G}_{\ell-1}^{-1} \mathbf{G}_\ell + (\nu_{\ell+1} - \nu_\ell) \mathbf{I}, \quad \text{for } \ell = 1, \dots, L. \quad (144)$$

Evaluating this expression for $\ell = 1$ and $\ell = 2$ gives,

$$\nu_2 \mathbf{G}_1^{-1} \mathbf{G}_2 = \nu_1 \mathbf{G}_0^{-1} \mathbf{G}_1 + (\nu_2 - \nu_1) \mathbf{I}, \quad (145)$$

$$\nu_3 \mathbf{G}_2^{-1} \mathbf{G}_3 = \nu_2 \mathbf{G}_1^{-1} \mathbf{G}_2 + (\nu_3 - \nu_2) \mathbf{I} = \nu_1 \mathbf{G}_0^{-1} \mathbf{G}_1 + (\nu_3 - \nu_1) \mathbf{I}. \quad (146)$$

Recurring, we get,

$$\nu_\ell \mathbf{G}_{\ell-1}^{-1} \mathbf{G}_\ell = \nu_1 \mathbf{G}_0^{-1} \mathbf{G}_1 + (\nu_\ell - \nu_1) \mathbf{I}. \quad (147)$$

Critically, this form highlights constraints on \mathbf{G}_1 . In particular, the right hand side, $\mathbf{G}_{\ell-1}^{-1} \mathbf{G}_\ell$, is the product of two positive definite matrices, so has positive eigenvalues (but may be non-symmetric [47]). Thus, all eigenvalues of $\nu_1 \mathbf{G}_0^{-1} \mathbf{G}_1$ must be larger than $\nu_1 - \nu_\ell$, and this holds true at all layers. This will become important later, as it rules out inadmissible solutions.

Given \mathbf{G}_0 and \mathbf{G}_1 , we can compute any \mathbf{G}_ℓ using,

$$\mathbf{G}_0^{-1} \mathbf{G}_\ell = \prod_{\ell'=1}^{\ell} (\mathbf{G}_{\ell'-1}^{-1} \mathbf{G}_{\ell'}) = \frac{1}{\prod_{\ell'=1}^{\ell} \nu_{\ell'}} \prod_{\ell'=1}^{\ell} (\nu_{\ell'} \mathbf{G}_{\ell'-1}^{-1} \mathbf{G}_{\ell'}) \quad (148)$$

$$\left(\prod_{\ell'=1}^{\ell} \nu_{\ell'} \right) \mathbf{G}_0^{-1} \mathbf{G}_\ell = \prod_{\ell'=1}^{\ell} (\nu_1 \mathbf{G}_0^{-1} \mathbf{G}_1 + (\nu_{\ell'} - \nu_1) \mathbf{I}) \quad (149)$$

where the matrix products are ordered as $\prod_{\ell=1}^L \mathbf{A}_\ell = \mathbf{A}_1 \cdots \mathbf{A}_L$. Now, we seek to solve for \mathbf{G}_1 using our knowledge of \mathbf{G}_{L+1} . Computing $\mathbf{G}_0^{-1} \mathbf{G}_{L+1}$,

$$\left(\prod_{\ell=1}^{L+1} \nu_\ell \right) \mathbf{G}_0^{-1} \mathbf{G}_{L+1} = \prod_{\ell=1}^{L+1} (\nu_1 \mathbf{G}_0^{-1} \mathbf{G}_1 + (\nu_\ell - \nu_1) \mathbf{I}). \quad (150)$$

We write the eigendecomposition of $\nu_1 \mathbf{G}_0^{-1} \mathbf{G}_1$ as,

$$\nu_1 \mathbf{G}_0^{-1} \mathbf{G}_1 = \mathbf{V} \mathbf{D} \mathbf{V}^{-1}. \quad (151)$$

Thus,

$$\left(\prod_{\ell=1}^{L+1} \nu_\ell \right) \mathbf{G}_0^{-1} \mathbf{G}_{L+1} = \prod_{\ell=1}^{L+1} (\mathbf{V} \mathbf{D} \mathbf{V}^{-1} + (\nu_\ell - \nu_1) \mathbf{I}) = \mathbf{V} \mathbf{\Lambda} \mathbf{V}^{-1} \quad (152)$$

where $\mathbf{\Lambda}$ is a diagonal matrix,

$$\mathbf{\Lambda} = \prod_{\ell=1}^{L+1} (\mathbf{D} + (\nu_\ell - \nu_1) \mathbf{I}). \quad (153)$$

Thus, we can identify \mathbf{V} and $\mathbf{\Lambda}$ by performing an eigendecomposition of the known matrix, $\left(\prod_{\ell=1}^{L+1} \nu_\ell \right) \mathbf{G}_0^{-1} \mathbf{G}_{L+1}$. Then, we can solve for \mathbf{D} (and hence \mathbf{G}_1) in terms of $\mathbf{\Lambda}$ and \mathbf{V} . The diagonal elements of \mathbf{D} satisfy,

$$0 = -\Lambda_{ii} + \prod_{k=1}^{L+1} (D_{ii} + (\nu_k - \nu_1)) \quad (154)$$

This is a polynomial, and remembering the constraints from Eq. (147), we are interested in solutions which satisfy,

$$\nu_1 - \nu_{\min} \leq D_{ii}. \quad (155)$$

where,

$$\nu_{\min} = \min(\nu_1, \dots, \nu_{L+1}) \quad (156)$$

To reason about the number of such solutions, we use Descartes' rule of signs, which states that the number of positive real roots is equal to or a multiple of two less than the number of sign changes in the coefficients of the polynomial. Thus, if there is one sign change, there must be one positive real root. For instance, in the following polynomial,

$$0 = x^3 + x^2 - 1 \quad (157)$$

the signs go as (+), (+), (-), so there is only one sign change, and there is one real root. To use Descartes' rule of signs, we work in terms of D'_{ii} , which is constrained to be positive,

$$0 \leq D'_{ii} = D_{ii} - (\nu_1 - \nu_{\min}) \quad D_{ii} = D'_{ii} + (\nu_1 - \nu_{\min}). \quad (158)$$

Thus, the polynomial of interest (Eq. 154) becomes,

$$0 = -\Lambda_{ii} + \prod_{\ell=1}^{L+1} (D'_{ii} + (\nu_1 - \nu_{\min}) - (\nu_1 - \nu_{\ell})) = -\Lambda_{ii} + \prod_{\ell=1}^{L+1} (D'_{ii} + (\nu_{\ell} - \nu_{\min})) \quad (159)$$

where $0 < \nu_{\ell} - \nu_{\min}$ as ν_{\min} is defined to be the smallest ν_{ℓ} (Eq. 156). Thus, the constant term, $-\Lambda_{ii}$ is negative, while all other terms, $D'_{ii}, \dots, (D'_{ii})^{L+1}$ in the polynomial have positive coefficients. Thus, there is only one sign change, which proves the existence of only one valid real root, as required.

J Unimodality experiments with nonlinear kernels

For the posterior over Gram matrices to converge to a point distribution, we need the DKM objective $\mathcal{L}(\mathbf{G}_1, \dots, \mathbf{G}_L)$ to have one unique global optimum. As noted above, this is guaranteed when the prior dominates (Eq. 12), and for linear models (Appendix I). While we believe that it might be possible to construct counter examples, in practice we expect a single global optimum in most practical settings. To confirm this expectation, we did a number of experiments, starting with many different random initializations of a deep kernel machine and optimizing using gradient descent (Appendix J). In all cases tested, the optimizers converged to the same maximum.

We parameterise Gram matrices $\mathbf{G}_{\ell} = \frac{1}{P} \mathbf{V}_{\ell} \mathbf{V}_{\ell}^T$ with $\mathbf{V}_{\ell} \in \mathbb{R}^{P \times P}$ being trainable parameters. To make initializations with different seeds sufficiently separated while ensuring stability we initialize \mathbf{G}_{ℓ} from a broad distribution that depends on $\mathbf{K}(\mathbf{G}_{\ell-1})$. Specifically, we first take the Cholesky decomposition $\mathbf{K}(\mathbf{G}_{\ell-1}) = \mathbf{L}_{\ell-1} \mathbf{L}_{\ell-1}^T$, then set $\mathbf{V}_{\ell} = \mathbf{L}_{\ell-1} \mathbf{\Xi}_{\ell} \mathbf{D}_{\ell}^{1/2}$ where each entry of $\mathbf{\Xi}_{\ell} \in \mathbb{R}^{P \times P}$ is independently sampled from a standard Gaussian, and \mathbf{D}_{ℓ} is a diagonal scaling matrix with each entry sampled i.i.d. from an inverse-Gamma distribution. The variance of the inverse-Gamma distribution is fixed to 100, and the mean is drawn from a uniform distribution $U[0.5, 3]$ for each seed. Since for any random variable $x \sim \text{Inv-Gamma}(\alpha, \beta)$, $\mathbb{E}(x) = \frac{\beta}{\alpha-1}$ and $\mathbb{V}(x) = \frac{\beta}{(\alpha-1)(\alpha-2)}$, once we fix the mean and variance we can compute α and β as

$$\alpha = \frac{\mathbb{E}(x)^2}{\mathbb{V}(x)} + 2, \quad (160)$$

$$\beta = \mathbb{E}(x)(\alpha - 1). \quad (161)$$

We set $\nu_{\ell} = 5$, and use the Adam optimizer [43] with learning rate 0.001 to optimize parameters \mathbf{V}_{ℓ} described above. We fixed all model hyperparameters to ensure that any multimodality could emerge only from the underlying deep kernel machine. As we did not use inducing points, we were forced to consider only the smaller UCI datasets (yacht, boston, energy and concrete). For the deep kernel machine objective, all Gram matrices converge rapidly to the same solution, as measured by RMSE (Fig. 12). Critically, we did find multiple modes for the MAP objective (Fig 13), indicating that experiments are indeed powerful enough to find multiple modes (though of course they cannot be guaranteed to find them). Finally, note that the Gram matrices took a surprisingly long time to converge: this was largely due to the high degree of diversity in the initializations; convergence was much faster if we initialised deterministically from the prior.

This might contradict our usual intuitions about huge multimodality in the weights/features of DNNs and DGPs. This can be reconciled by noting that each mode, written in terms of Gram matrices,

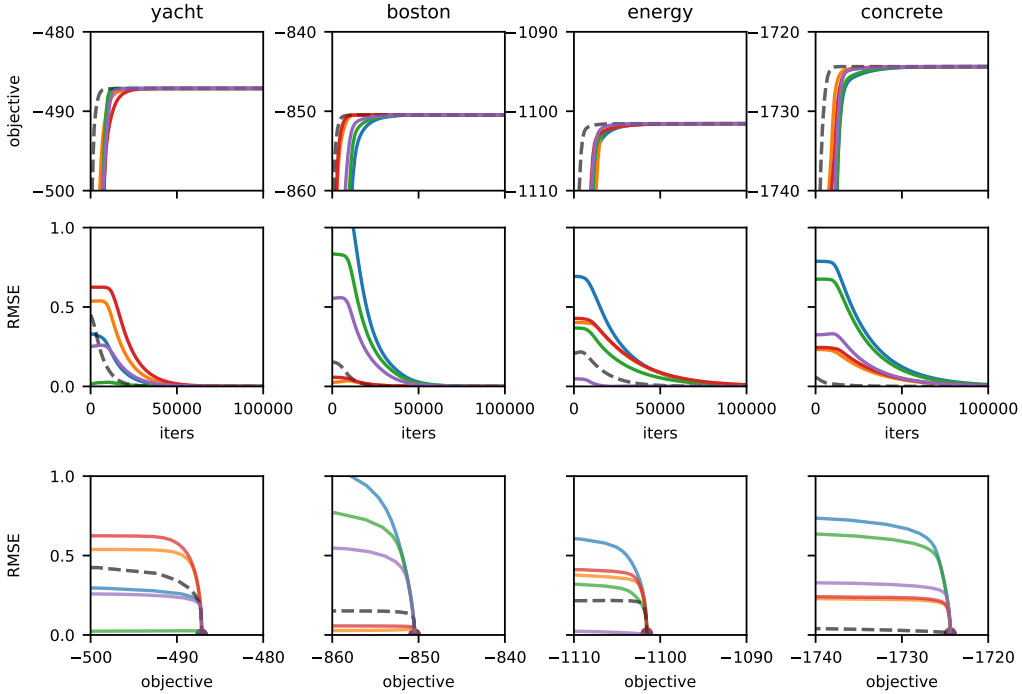


Figure 12: One-layer DKMs with squared exponential kernel trained on full UCI datasets (through columns) converges to the same solution, despite very different initializations by applying stochastic diagonal scalings described in the Method section to the standard initialization with different seeds. Standard initialization is shown in dashed line, while scaled initializations are the color lines each denoting a different seed. The first row shows the objective during training for all seeds that all converge to the same value. The second row shows the element-wise RMSE between the Gram matrix of each seed and the optimized Gram matrix obtained from the standard initialization. RMSE converges to 0 as all initializations converge on the same maximum. The last row plots RMSE versus objective value, again showing a single optimal objective value where all Gram matrices are the same.

corresponds to (perhaps infinitely) many modal features. In particular, in Sec. E.1, we show that the log-probability for features, $P(\mathbf{F}_\ell | \mathbf{F}_{\ell-1})$ (Eq. 83) depends only on the Gram matrices, and note that there are many settings of features which give the same Gram matrix. In particular, the Gram matrix is the same for any unitary transformation of the features, $\mathbf{F}'_\ell = \mathbf{F}_\ell \mathbf{U}$, satisfying $\mathbf{U}\mathbf{U}^T = \mathbf{I}$, as $\frac{1}{N_\ell} \mathbf{F}'_\ell \mathbf{F}'_\ell{}^T = \frac{1}{N_\ell} \mathbf{F}_\ell \mathbf{U} \mathbf{U}^T \mathbf{F}_\ell^T = \frac{1}{N_\ell} \mathbf{F}_\ell \mathbf{F}_\ell^T = \mathbf{G}_\ell$. For DGPs we can use any unitary matrix, so there are infinitely many sets of features consistent with a particular Gram matrix, while for DNNs we can only use permutation matrices, which are a subset of unitary matrices. Thus, the objective landscape must be far more complex in the feature domain than with Gram matrices, as a single optimal Gram matrix corresponds to a large family of optimal features.

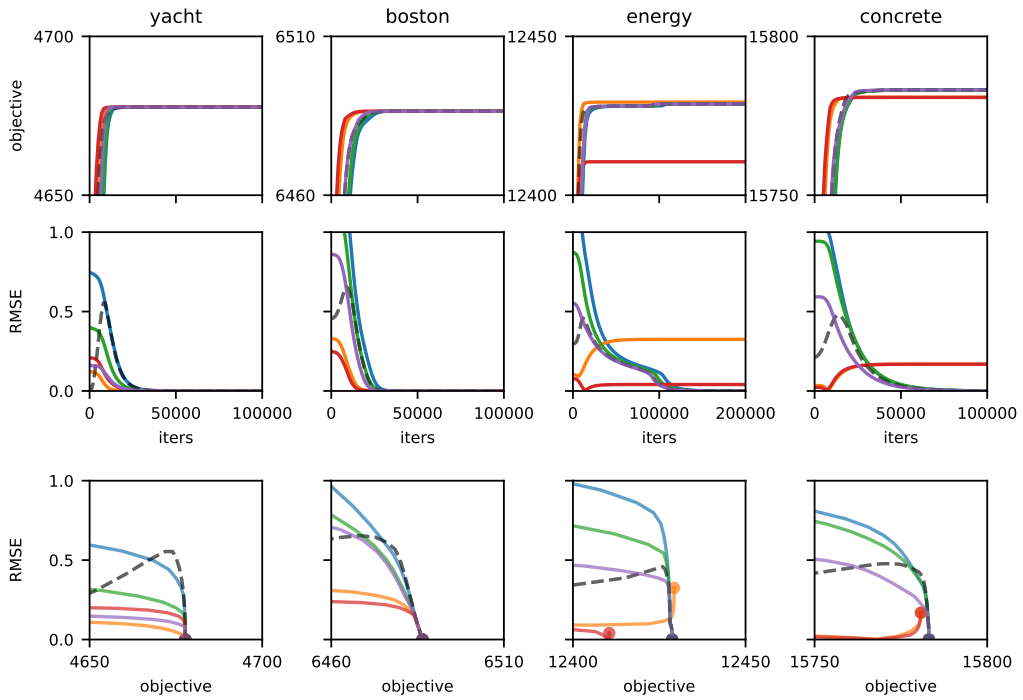


Figure 13: One-layer DKM with MAP inference over features as described in Appendix E.1 Eq. (85). Rows and columns are the same as in Figure 12. Using the same randomly scaled initializations described above, we are able to find multiple modes in energy and concrete showing our initializations are diverse enough, albeit there is still only a single global optimum.

K Inducing point DKMs

To do large-scale experiments on UCI datasets, we introduce inducing point DKMs by extending Gaussian process inducing point methods [34] to the DKM setting. This approach uses the variational interpretation of the deep kernel machine objective described in Appendix D.

To do inducing-point variational inference, we need to explicitly introduce top-layer features mirroring $\mathbf{F}_{L+1} \in \mathbb{R}^{P \times \nu_{L+1}}$ in Appendix A, but replicated N times, $\tilde{\mathbf{F}}_{L+1} \in \mathbb{R}^{P \times N_{L+1}}$. Formally, each feature, $\tilde{\mathbf{f}}_1^{L+1}, \dots, \tilde{\mathbf{f}}_{N_{L+1}}^{L+1}$ is IID, conditioned on \mathbf{F}_L ,

$$P(\tilde{\mathbf{F}}_{L+1} | \mathbf{F}_L) = \prod_{\lambda=1}^{N_\ell} \mathcal{N}(\tilde{\mathbf{f}}_\lambda^{L+1}; \mathbf{0}, \mathbf{K}(\mathbf{G}(\mathbf{F}_L))), \quad (162a)$$

$$P(\tilde{\mathbf{Y}} | \tilde{\mathbf{F}}_{L+1}) = \prod_{\lambda=1}^{N_\ell} \mathcal{N}(\tilde{\mathbf{y}}_\lambda; \tilde{\mathbf{f}}_\lambda^{L+1}, \sigma^2 \mathbf{I}). \quad (162b)$$

where we give the likelihood for regression, but other likelihoods (e.g. for classification) are possible (Appendix A).

Further, we take the total number of points, P , to be made up of P_i inducing points and P_t test/train points, so that $P = P_i + P_t$. Thus, we can separate all features, $\mathbf{F}_\ell \in \mathbb{R}^{N_\ell \times P}$, into the inducing features, $\mathbf{F}_i^\ell \in \mathbb{R}^{N_\ell \times P_i}$, and the test/train features, $\mathbf{F}_t^\ell \in \mathbb{R}^{N_\ell \times P_t}$. Likewise, we separate the inputs, \mathbf{X} , and outputs, \mathbf{Y} , into (potentially trained) inducing inputs, \mathbf{X}_i , and trained inducing outputs, \mathbf{Y}_i , and the real test/training inputs, \mathbf{X}_t , and outputs, \mathbf{Y}_t ,

$$\mathbf{F}_\ell = \begin{pmatrix} \mathbf{F}_i^\ell \\ \mathbf{F}_t^\ell \end{pmatrix} \quad \tilde{\mathbf{F}}_{L+1} = \begin{pmatrix} \tilde{\mathbf{F}}_i^{L+1} \\ \tilde{\mathbf{F}}_t^{L+1} \end{pmatrix} \quad \mathbf{X} = \begin{pmatrix} \mathbf{X}_i \\ \mathbf{X}_t \end{pmatrix} \quad \mathbf{Y} = \begin{pmatrix} \mathbf{Y}_i \\ \mathbf{Y}_t \end{pmatrix} \quad \tilde{\mathbf{Y}} = \begin{pmatrix} \tilde{\mathbf{Y}}_i \\ \tilde{\mathbf{Y}}_t \end{pmatrix} \quad (163)$$

We follow the usual doubly stochastic inducing point approach for DGPs. In particular, we treat all the features at intermediate layers, $\mathbf{F}_1, \dots, \mathbf{F}_L$, and the top-layer train/test features, \mathbf{F}_t^{L+1} as latent variables. However, we deviate from the usual setup in treating the top-layer inducing outputs, \mathbf{F}_i^{L+1} , as learned parameters and maximize over them to ensure that the ultimate method does not require sampling, and at the same time allows minibatched training. The prior and approximate posterior over $\mathbf{F}_1, \dots, \mathbf{F}_L$ are given by,

$$Q(\mathbf{F}_1, \dots, \mathbf{F}_L | \mathbf{X}) = \prod_{\ell=1}^L Q(\mathbf{F}_\ell | \mathbf{F}_{\ell-1}), \quad (164a)$$

$$P(\mathbf{F}_1, \dots, \mathbf{F}_L | \mathbf{X}) = \prod_{\ell=1}^L P(\mathbf{F}_\ell | \mathbf{F}_{\ell-1}), \quad (164b)$$

and remember $\mathbf{F}_0 = \mathbf{X}$, so $\mathbf{G}_0 = \frac{1}{N_0} \mathbf{X} \mathbf{X}^T$. The prior and approximate posterior at each layer factorises into a distribution over the inducing points and a distribution over the test/train points,

$$Q(\mathbf{F}_\ell | \mathbf{F}_{\ell-1}) = P(\mathbf{F}_t^\ell | \mathbf{F}_i^\ell, \mathbf{F}_{\ell-1}) Q(\mathbf{F}_i^\ell), \quad (165a)$$

$$P(\mathbf{F}_\ell | \mathbf{F}_{\ell-1}) = P(\mathbf{F}_t^\ell | \mathbf{F}_i^\ell, \mathbf{F}_{\ell-1}) P(\mathbf{F}_i^\ell | \mathbf{F}_i^{\ell-1}). \quad (165b)$$

Critically, the approximate posterior samples for the test/train points is the conditional prior $P(\mathbf{F}_t^\ell | \mathbf{F}_i^\ell, \mathbf{F}_{\ell-1})$, which is going to lead to cancellation when we compute the ELBO. Likewise, the approximate posterior over $\tilde{\mathbf{F}}_t^{L+1}$ is the conditional prior,

$$Q(\tilde{\mathbf{F}}_t^{L+1} | \mathbf{F}_i^{L+1}, \mathbf{F}_L) = P(\tilde{\mathbf{F}}_t^{L+1} | \mathbf{F}_i^{L+1}, \mathbf{F}_L). \quad (166)$$

Concretely, the prior approximate posterior over inducing points are given by,

$$Q(\mathbf{F}_i^\ell) = \prod_{\lambda=1}^{N_\ell} \mathcal{N}(\mathbf{f}_{i,\lambda}^\ell; \mathbf{0}, \mathbf{G}_{ii}^\ell), \quad (167a)$$

$$P(\mathbf{F}_i^\ell | \mathbf{F}_i^{\ell-1}) = \prod_{\lambda=1}^{N_\ell} \mathcal{N}(\mathbf{f}_{i,\lambda}^\ell; \mathbf{0}, \mathbf{K}(\mathbf{G}(\mathbf{F}_i^{\ell-1}))) \quad (167b)$$

The approximate posterior is directly analogous to Eq. (71) and the prior is directly analogous to Eq. (1a), but where we have specified that this is only over inducing points. Now we compute the ELBO

$$\begin{aligned} & \text{ELBO}(\mathbf{F}_i^{L+1}, \mathbf{G}_{ii}^1, \dots, \mathbf{G}_{ii}^L) \\ &= \mathbb{E}_Q \left[\log P(\tilde{\mathbf{Y}}_t | \tilde{\mathbf{F}}_t^{L+1}) + \log \frac{P(\tilde{\mathbf{F}}_t^{L+1} | \mathbf{F}_i^{L+1}, \mathbf{F}_L) P(\mathbf{F}_1, \dots, \mathbf{F}_L | \mathbf{X})}{Q(\tilde{\mathbf{F}}_t^{L+1} | \mathbf{F}_i^{L+1}, \mathbf{F}_L) Q(\mathbf{F}_1, \dots, \mathbf{F}_L | \mathbf{X})} \right] \quad (168) \end{aligned}$$

Note that the $P(\mathbf{F}_t^\ell | \mathbf{F}_i^\ell, \mathbf{F}_{\ell-1})$ terms are going to cancel in the ELBO, we consider them below when we come to describing sampling), substituting Eq. (164–166) and cancelling $P(\mathbf{F}_t^\ell | \mathbf{F}_i^\ell, \mathbf{F}_{\ell-1})$ and $P(\tilde{\mathbf{F}}_t^{L+1} | \mathbf{F}_i^{L+1}, \mathbf{F}_L)$,

$$\text{ELBO}(\mathbf{F}_i^{L+1}, \mathbf{G}_{\text{ii}}^1, \dots, \mathbf{G}_{\text{ii}}^L) = \mathbb{E}_{\mathbf{Q}} \left[\log P(\tilde{\mathbf{Y}}_t | \tilde{\mathbf{F}}_t^{L+1}) + \sum_{\ell=1}^L \log \frac{P(\mathbf{F}_i^\ell | \mathbf{F}_i^{\ell-1})}{Q(\mathbf{F}_i^\ell)} \right]. \quad (169)$$

So far, we have treated the Gram matrices, $\mathbf{G}_{\text{ii}}^\ell$ as parameters of the approximate posterior. However, in the infinite limit $N \rightarrow \infty$, these are consistent with the features generated by the approximate posterior. In particular the matrix product $\frac{1}{N_\ell} \mathbf{F}_i^\ell (\mathbf{F}_i^\ell)^T$ can be written as an average over infinitely many IID vectors, $\mathbf{f}_{i;\lambda}^\ell$ (first equality), and by the law of large numbers, this is equal to the expectation of one term (second equality), which is $\mathbf{G}_{\text{ii}}^\ell$ (by the approximate posterior Eq. (167a)),

$$\lim_{N \rightarrow \infty} \frac{1}{N_\ell} \mathbf{F}_i^\ell (\mathbf{F}_i^\ell)^T = \lim_{N \rightarrow \infty} \frac{1}{N_\ell} \sum_{\lambda=1}^{N_\ell} \mathbf{f}_{i;\lambda}^\ell (\mathbf{f}_{i;\lambda}^\ell)^T = \mathbb{E}_{\mathbf{Q}(\mathbf{f}_{i;\lambda}^\ell)} \left[\mathbf{f}_{i;\lambda}^\ell (\mathbf{f}_{i;\lambda}^\ell)^T \right] = \mathbf{G}_{\text{ii}}^\ell. \quad (170)$$

By this argument, the Gram matrix from the previous layer, $\mathbf{G}_{\text{ii}}^{\ell-1}$ is deterministic. Further, in a DGP, \mathbf{F}_i^ℓ only depends on $\mathbf{F}_i^{\ell-1}$ through $\mathbf{G}_i^{\ell-1}$ (Eq. 6), and the prior and approximate posterior factorise. Thus, in the infinite limit, individual terms in the ELBO can be written,

$$\lim_{N \rightarrow \infty} \frac{1}{N} \mathbb{E}_{\mathbf{Q}} \left[\log \frac{P(\mathbf{F}_i^\ell | \mathbf{F}_i^{\ell-1})}{Q(\mathbf{F}_i^\ell)} \right] = \nu_\ell \mathbb{E}_{\mathbf{Q}} \left[\log \frac{P(\mathbf{f}_{i;\lambda}^\ell | \mathbf{G}_i^{\ell-1})}{Q(\mathbf{f}_{i;\lambda}^\ell)} \right] \quad (171)$$

$$= -\nu_\ell \text{D}_{\text{KL}}(\mathcal{N}(\mathbf{0}, \mathbf{K}(\mathbf{G}_i^{\ell-1})) \| \mathcal{N}(\mathbf{0}, \mathbf{G}_i^\ell)). \quad (172)$$

where the final equality arises when we notice that the expectation can be written as a KL-divergence. The inducing DKM objective, \mathcal{L}_{ind} , is the ELBO, divided by N to ensure that it remains finite in the infinite limit,

$$\begin{aligned} \mathcal{L}_{\text{ind}}(\mathbf{F}_i^{L+1}, \mathbf{G}_{\text{ii}}^1, \dots, \mathbf{G}_{\text{ii}}^L) &= \lim_{N \rightarrow \infty} \frac{1}{N} \text{ELBO}(\mathbf{F}_i^{L+1}, \mathbf{G}_{\text{ii}}^1, \dots, \mathbf{G}_{\text{ii}}^L) \\ &= \mathbb{E}_{\mathbf{Q}} \left[\log P(\mathbf{Y}_t | \mathbf{F}_t^{L+1}) \right] - \sum_{\ell=1}^L \nu_\ell \text{D}_{\text{KL}}(\mathcal{N}(\mathbf{0}, \mathbf{K}(\mathbf{G}_{\text{ii}}^{\ell-1})) \| \mathcal{N}(\mathbf{0}, \mathbf{G}_{\text{ii}}^\ell)). \end{aligned} \quad (173)$$

Note that this has almost exactly the same form as the standard DKM objective for DGPs in the main text (Eq. 17). In particular, the second term is a chain of KL-divergences, with the only difference that these KL-divergences apply only to the inducing points. The first term is a “performance” term that here depends on the quality of the predictions given the inducing points. As the copies are IID, we have,

$$\mathbb{E}_{\mathbf{Q}} \left[\log P(\tilde{\mathbf{Y}}_t | \tilde{\mathbf{F}}_t^{L+1}) \right] = N \mathbb{E}_{\mathbf{Q}} \left[\log P(\mathbf{Y}_t | \mathbf{F}_t^{L+1}) \right]. \quad (174)$$

Now that we have a simple form for the ELBO, we need to compute the expected likelihood, $\mathbb{E}_{\mathbf{Q}} \left[\log P(\mathbf{Y}_t | \mathbf{F}_t^{L+1}) \right]$. This requires us to compute the full Gram matrices, including test/train points, conditioned on the optimized inducing Gram matrices. We start by defining the full Gram matrix,

$$\mathbf{G}_\ell = \begin{pmatrix} \mathbf{G}_{\text{ii}}^\ell & \mathbf{G}_{\text{it}}^\ell \\ \mathbf{G}_{\text{ti}}^\ell & \mathbf{G}_{\text{tt}}^\ell \end{pmatrix} \quad (175)$$

for both inducing points (labelled “i”) and test/training points (labelled “t”) from just $\mathbf{G}_{\text{ii}}^\ell$. For clarity, we have $\mathbf{G}_\ell \in \mathbb{R}^{P \times P}$, $\mathbf{G}_{\text{ii}}^\ell \in \mathbb{R}^{P_i \times P_i}$, $\mathbf{G}_{\text{ti}}^\ell \in \mathbb{R}^{P_i \times P_t}$, $\mathbf{G}_{\text{tt}}^\ell \in \mathbb{R}^{P_t \times P_t}$, where P_i is the number of inducing points, P_t is the number of train/test points and $P = P_i + P_t$ is the total number of inducing and train/test points.

The conditional distribution over \mathbf{F}_t^ℓ given \mathbf{F}_i^ℓ is,

$$P(\mathbf{F}_t^\ell | \mathbf{F}_i^\ell, \mathbf{G}_{\ell-1}) = \prod_{\lambda=1}^{N_\ell} \mathcal{N}(\mathbf{f}_{t;\lambda}^\ell; \mathbf{K}_{\text{ti}} \mathbf{K}_{\text{ii}}^{-1} \mathbf{f}_{i;\lambda}^\ell, \mathbf{K}_{\text{tt}}) \quad (176)$$

Algorithm 1 DKM prediction

Parameters: $\{\nu_\ell\}_{\ell=1}^L$
Optimized Gram matrices $\{\mathbf{G}_{ii}^\ell\}_{\ell=1}^L$
Inducing and train/test inputs: $\mathbf{X}_i, \mathbf{X}_t$
Inducing outputs: \mathbf{F}_i^{L+1}

Initialize full Gram matrix

$$\begin{pmatrix} \mathbf{G}_{ii}^0 & \mathbf{G}_{ti}^{0:T} \\ \mathbf{G}_{ti}^0 & \mathbf{G}_{tt}^0 \end{pmatrix} = \frac{1}{\nu_0} \begin{pmatrix} \mathbf{X}_i \mathbf{X}_i^T & \mathbf{X}_i \mathbf{X}_t^T \\ \mathbf{X}_t \mathbf{X}_i^T & \mathbf{X}_t \mathbf{X}_t^T \end{pmatrix}$$

Propagate full Gram matrix

for ℓ **in** $(1, \dots, L)$ **do**

$$\begin{pmatrix} \mathbf{K}_{ii} & \mathbf{K}_{ti}^T \\ \mathbf{K}_{ti} & \mathbf{K}_{tt} \end{pmatrix} = \mathbf{K} \left(\begin{pmatrix} \mathbf{G}_{ii}^{\ell-1} & (\mathbf{G}_{ti}^{\ell-1})^T \\ \mathbf{G}_{ti}^{\ell-1} & \mathbf{G}_{tt}^{\ell-1} \end{pmatrix} \right)$$

$$\mathbf{K}_{t:i} = \mathbf{K}_{tt} - \mathbf{K}_{ti} \mathbf{K}_{ii}^{-1} \mathbf{K}_{ti}^T.$$

$$\mathbf{G}_{ii}^\ell = \mathbf{K}_{ii} \mathbf{K}_{ii}^{-1} \mathbf{G}_{ii}^\ell$$

$$\mathbf{G}_{tt}^\ell = \mathbf{K}_{ti} \mathbf{K}_{ii}^{-1} \mathbf{G}_{ii}^\ell \mathbf{K}_{ii}^{-1} \mathbf{K}_{ti}^T + \mathbf{K}_{t:i}$$

end for

Final prediction using standard Gaussian process expressions

$$\begin{pmatrix} \mathbf{K}_{ii} & \mathbf{K}_{ti}^T \\ \mathbf{K}_{ti} & \mathbf{K}_{tt} \end{pmatrix} = \mathbf{K} \left(\begin{pmatrix} \mathbf{G}_{ii}^L & (\mathbf{G}_{ti}^L)^T \\ \mathbf{G}_{ti}^L & \mathbf{G}_{tt}^L \end{pmatrix} \right)$$

$$\mathbf{Y}_t \sim \mathcal{N}(\mathbf{K}_{ti} \mathbf{K}_{ii}^{-1} \mathbf{F}_i^{L+1}, \mathbf{K}_{t:i} - \mathbf{K}_{ti} \mathbf{K}_{ii}^{-1} \mathbf{K}_{ti}^T + \sigma^2 \mathbf{I})$$

where $\mathbf{f}_{t;\lambda}^\ell$ is the activation of the λ th feature for all train/test inputs, $\mathbf{f}_{i;\lambda}^\ell$ is the activation of the λ th feature for all train/test inputs, and $\mathbf{f}_{i;\lambda}^\ell$, and

$$\begin{pmatrix} \mathbf{K}_{ii} & \mathbf{K}_{ti}^T \\ \mathbf{K}_{ti} & \mathbf{K}_{tt} \end{pmatrix} = \mathbf{K} \left(\frac{1}{N_{\ell-1}} \mathbf{F}_{\ell-1} \mathbf{F}_{\ell-1}^T \right) = \mathbf{K}(\mathbf{G}_{\ell-1}) \quad (177)$$

$$\mathbf{K}_{t:i} = \mathbf{K}_{tt} - \mathbf{K}_{ti} \mathbf{K}_{ii}^{-1} \mathbf{K}_{ti}^T. \quad (178)$$

In the infinite limit, the Gram matrix becomes deterministic via the law of large numbers (as in Eq. 170), and as such \mathbf{G}_{ii} and \mathbf{G}_{tt} become deterministic and equal to their expected values. Using Eq. (176), we can write,

$$\mathbf{F}_t^\ell = \mathbf{K}_{ti} \mathbf{K}_{ii}^{-1} \mathbf{F}_i^\ell + \mathbf{K}_{t:i}^{1/2} \mathbf{\Xi}. \quad (179)$$

where $\mathbf{\Xi}$ is a matrix with IID standard Gaussian elements. Thus,

$$\mathbf{G}_{ii}^\ell = \frac{1}{\nu} \mathbb{E} [\mathbf{F}_t^\ell (\mathbf{F}_t^\ell)^T] \quad (180)$$

$$= \frac{1}{\nu} \mathbf{K}_{ti} \mathbf{K}_{ii}^{-1} \mathbb{E} [\mathbf{F}_i^\ell (\mathbf{F}_i^\ell)^T] \quad (181)$$

$$= \mathbf{K}_{ti} \mathbf{K}_{ii}^{-1} \mathbf{G}_{ii}^\ell \quad (182)$$

and,

$$\mathbf{G}_{tt}^\ell = \frac{1}{\nu} \mathbb{E} [\mathbf{F}_t^\ell (\mathbf{F}_t^\ell)^T] \quad (183)$$

$$= \frac{1}{\nu} \mathbf{K}_{ti} \mathbf{K}_{ii}^{-1} \mathbb{E} [\mathbf{F}_i^\ell (\mathbf{F}_i^\ell)^T] \mathbf{K}_{ii}^{-1} \mathbf{K}_{ti}^T + \frac{1}{\nu} \mathbf{K}_{t:i}^{1/2} \mathbb{E} [\mathbf{\Xi} \mathbf{\Xi}^T] \mathbf{K}_{t:i}^{1/2} \quad (184)$$

$$= \mathbf{K}_{ti} \mathbf{K}_{ii}^{-1} \mathbf{G}_{ii}^\ell \mathbf{K}_{ii}^{-1} \mathbf{K}_{ti}^T + \mathbf{K}_{t:i} \quad (185)$$

For the full prediction algorithm, see Alg. 1.